Summer 1998

The optimized electrostatic motor

Christopher Lee Rambin
Louisiana Tech University

INFORMATION TO USERS

This manuscript has been reproduced from the microfilm master. UMI films the text directly from the original or copy submitted. Thus, some thesis and dissertation copies are in typewriter face, while others may be from any type of computer printer.

The quality of this reproduction is dependent upon the quality of the copy submitted. Broken or indistinct print, colored or poor quality illustrations and photographs, print bleedthrough, substandard margins, and improper alignment can adversely affect reproduction.

In the unlikely event that the author did not send UMI a complete manuscript and there are missing pages, these will be noted. Also, if unauthorized copyright material had to be removed, a note will indicate the deletion.

Oversize materials (e.g., maps, drawings, charts) are reproduced by sectioning the original, beginning at the upper left-hand corner and continuing from left to right in equal sections with small overlaps. Each original is also photographed in one exposure and is included in reduced form at the back of the book.

Photographs included in the original manuscript have been reproduced xerographically in this copy. Higher quality 6" x 9" black and white photographic prints are available for any photographs or illustrations appearing in this copy for an additional charge. Contact UMI directly to order.

UMI

A Bell & Howell Information Company
300 North Zeeb Road, Ann Arbor MI 48106-1346 USA
313/761-4700 800/521-0600

THE OPTIMIZED ELECTROSTATIC MOTOR

by

Christopher Lee Rambin

A Dissertation Presented in Partial Fulfillment
of the Requirements for the Degree
Doctor of Engineering

COLLEGE OF ENGINEERING AND SCIENCE
LOUISIANA TECH UNIVERSITY

May, 1998

LOUISIANA TECH UNIVERSITY

THE GRADUATE SCHOOL

May 26, 1998
Date

We hereby recommend that the Dissertation prepared under our supervision by Christopher Lee Rambin

entitled The Optimized Electrostatic Motor

be accepted in partial fulfillment of the requirements for the Degree of Doctor of Engineering

William Jordan
Supervisor of Thesis Research

James D. Lawther
Head of Department

Mechanical Engineering
Department

Recommendation concurred in:

James D. Lawther

Lars E. Rolness

E. Eugene Fallen, Jr.

Advisory Committee

Approved:

James D. Nelson
Director of Graduate Studies

Leslie K. Quick
Dean of the College

Approved:

T. McConathy
Dean of Graduate School

ABSTRACT

The most common means of electrically activated actuation is the electromagnetic motor. All electromagnetic motors have a low output to weight ratio and low energy efficiency. The motor's weight is due to the coils and magnets used to generate propulsion. The energy loss is mainly the result of Joule heating that is inherent with any current driven device. An electrostatic motor offers the potential of significantly less weight and higher energy efficiency. This lower weight characteristic is due to the epoxide material used to construct the major components of its propulsion unit. Greater efficiency results from the reduced Joule heating since it is propelled by voltage induced charging which requires only small current pulses.

Electrostatic motors have not been successful in the past because the fabrication methods for producing very small electrodes in light-weight materials were not available. As the methods for construction of the ultra-fine electrodes necessary for sufficient torque became common, another problem arose due to the presumption of arbitrary values for the design parameters. Since methods for manufacturing microstructures are now commercially available, the remaining challenge is to systematically vary the fabrication parameters to discover the best possible design of an electrostatic motor that could possibly deliver the same torque as an electromagnetic motor but has less weight and uses less energy to perform the same amount of work.

Using the COULOMB program for the numerical analysis of the electrostatically induced torque between the motor's electrodes, a design optimization process has been established. By following this method for a fixed set of fabrication parameters, the electrode pattern that produces the highest torque or greatest work per revolution can be found. An example is given to show that when the design parameters are chosen randomly, the resulting electrode pattern generates torque that is less than half the optimum value. By evaluating the combined effect of stacking the flat stator-rotor pairs into the housing of an electromagnetic motor, the total predicted output torque from an optimized electrostatic motor is shown to match that delivered by the electromagnetic motor selected for comparison. Thus, an optimized rotary electrostatically driven actuator has the potential to replace the electromagnetic motor as the preferred means of electrically induced motion.

TABLE OF CONTENTS

ABSTRACT iii

LIST OF TABLES x

LIST OF FIGURES xi

INTRODUCTION 1

Early Electrostatic Motors 2

Fabrication and Circuit Limitations 5

Precision Machining 5

The Power Supply 6

Variable Capacitance Motors 7

Recent Electrostatic Motor Designs 8

The Macro Motors 8

The Micromotors 10

Success with a Linear Electrostatic Actuator 12

New Conductors 13

The State of the Art 13

CHAPTER 1

THE ELECTROSTATIC MOTOR DESIGN BASICS 14

Edge and Surface Drive 14

Parametric Variations Affecting the
Performance of an Electrostatic Motor 15

Fabrication Width 16

The Number of Electrode Groups 16

The Electrode Shape 19

The Stator and Rotor Separation Distance 20

The Controller / Driver 21

Rotational Speed and External Load Limits 22

CHAPTER 2

ACTUATOR PARAMETERS 23

The Linear Actuator 24

The Actuator Housing 25

The Stator and Slider 26

The Propulsion Stack 28

The Electrode Pattern 31

The Rotary Actuator 32

The Motor Housing 32

The Stator, Rotor, and Shaft 33

The Propulsion Stack 35

The Electrode Pattern 36

The Electrode Shape 37

Parameter Lists 39

CHAPTER 3

THE MOTION EQUATIONS 41

Formulation of the Linear Models 41

The Line Integral Method 41

The Surface Integral Method 45

Formulation of the Rotary Models 46

The Line Integral Method 46

The Surface Integral Method 49

An Alternative Form of the Electric Potential 54

The General Torque Equation 55

The Boundary Element Method 57

Analysis of the AT&T Motor 59

The Rotation Rate Equation 63

CHAPTER 4

THE OPTIMIZATION AND DESIGN PROCESSES 65

The Optimization Criteria for a Linear Electrostatic Actuator 65

The Optimization Process for a Rotary Actuator 67

The Design Procedure for a Linear Electrostatic Actuator 69

The Design Procedure for a Rotary Actuator 71

CHAPTER 5

A NUMERICAL OPTIMIZATION EXAMPLE 74

The Design Procedure for a Rotary Actuator 75

The Optimization Process for a Rotary Actuator 78

The Output Comparison 82

CHAPTER 6

DATA ANALYSIS AND METHODOLOGY 83

Model 5-50-30: Ro= 5 mm, s = 50 μm, z = 30 μm 84

The Electrode Shape Angle Effects 90

The Vertical Gap Effect 92

Optimization with the Shape Angle Effect 94

Model 5-100-50: Ro= 5 mm, s = 100 μm, z = 50 μm 95

The Difference between Charge Patterns 98

Model 5-75-40: Ro= 5 mm, s = 75 μm, z = 50 μm 99

Model 5-25-20: Ro= 5 mm, s = 25 μm, z = 20 μm 101

Model 2.5-25-15: Ro= 2.5 mm, s = 25 μm, z = 15 μm 103

Combination of 5 mm Radius Model Data 104

The AT&T Model 105

CONCLUSION 106

REFERENCES 107

LIST OF TABLES

1. Defined Shape Angles 38

2. Linear Parameter Summary 39

3. Summary of Rotary Parametric Relations 39

4. Rotary Parameter Summary 40

5. Input Parameters for Steps 3 to 8 79

6. Input Parameters for Steps 9 to 11 80

7. Model Parameters 83

8. Normalized Peak Data Points 89

LIST OF FIGURES

1. Example of the Edge Drive and Surface Drive Electrode Patterns 15

2. Example of Possible Electrode Patterns 17

3. Transition from the First to the Second Electrode Pattern 18

4. Transition from the Last to the Previous Electrode Pattern 18

5. Graphical Representation for Finding the Peak Torque 19

6. Outer View of a Linear Actuator 25

7. Propulsion Unit Dimensions 25

8. A Single Slider Board 26

9. Slider and Stator End Mounts 27

10. Cross-Section of a Base Board 27

11. Stack of Stators and Sliders 29

12. An Electrode Group 31

13. Outer View of an Electromagnetic Motor 32

14. Dimensions for Motor Cavity 33

15. The Stator and Rotor Boards 34

16. The Rotor Shaft 34

17. The Propulsion Stack 35

18. The Electrode Base 36

19. An Electrode Group 36
20. The Electrode Shapes 38
21. Capacitance Parameters 42
22. Linear Model Variables 43
23. The Line Charge Variables 47
24. Radial Variables 48
25. Surface Integral Spatial Variables 49
26. Integration Element Variables 50
27. Wedge Shaped Electrode 50
28. Representation of Charged Electrode Groups 52
29. Coarse Torque Data 79
30. Refined Torque Data 80
31. Optimum Electrode Pattern 81
32. Coarse Torque Data 84
33. Torque versus Rotor Position 85
34. Torque Plot at 60% Rotation 86
35. The Work per Revolution Data 86
36. Refined Torque Data for the Initial Rotor Position 87
37. Refined Torque Data for 60% Rotation 87
38. Refined Work per Revolution Data 88
39. Normalized Output Data 88
40. Shape Angle Curves 90

41. Peak Torque and Maximum Area Curves 91
42. Shape Angle Effect on Work per Revolution 91
43. Effect of Gap Distance on Torque 92
44. Work per Revolution Data 93
45. Shift in Optimum Electrode Pattern 94
46. Torque Data of Initial Rotor Position 95
47. Torque Data for 60% Rotation 96
48. Extended Torque Data 96
49. Torque Data for 60% Rotation Case 97
50. Torque Data for Wider Electrode 98
51. Comparison of Charge Pattern Effects 99
52. Torque Data for 60% Rotation Case 99
53. Torque Data for the Wider Electrode 100
54. Work Data for the Wider Electrode 100
55. Coarse Torque Data 101
56. Refined Torque Data 101
57. Coarse Work per Revolution Data 102
58. Refined Work per Revolution Data 102
59. Coarse Torque Data 103
60. Refined Torque Data 103
61. Combined Torque Data 104
62. Torque Data for the AT&T Model 105

INTRODUCTION

The purpose of all electrical motors is the transfer of electrical energy into mechanical work. The means of transfer has evolved into either a purely electric or an electromagnetic means. Limitations in the methods for fabrication and the design of electrostatic motors have restricted their output giving the electromagnetic method of propulsion a clear advantage. All electromagnetic motors suffer from the confines of excessive weight and high energy loss due to Joule heating. However, without a comparable competitor, electromagnetic motors have been accepted world wide as the only practical electrically operated source for rotational power.

For the same volume and output as electromagnetic motors, the electrostatic type offers the advantages of less weight and greater energy efficiency. The weight reduction is due to the materials used to construct the stator layers that form the means of propulsion. Electromagnetic motors require wire coils for the electric components and iron cores for the magnetic components. Electrostatic motors use thin epoxide layers to form both the stator and rotors. The weight density of these epoxide layers is far less than the density of the copper and iron used in electromagnetic motors. Energy loss in the electrostatic motors is inherently less than electromagnet because the former is driven by static charge delivered by small current pulses while the latter relies on the Lorentz force produced by sinusoidal

current. The low current of the static case causes less Joule heating than the much higher current for the magnetic case.

Past electrostatic motor designers have lacked the recognition that among the parametric variations of the electrode pattern, an optimum arrangement exists that will yield the maximum possible torque for any given voltage input. Failure to choose the right pattern has left past motors with a peak torque that was far less than the maximum value predicted by the optimum design. With the best possible motor design constructed using modern micro mechanical fabrication methods, a light-weight and energy efficient electrostatic motor can now be produced with its mechanical output sufficient to compete with electromagnet motors.

Early Electrostatic Motors

Among the first recorded motion devices that employed electricity as a means of propulsion is a rotary machine built by Benjamin Franklin in 1748[1]. The motor consisted of small metallic spheres at the ends of glass rods set in a radial pattern with a vertical axis. Two spheres mounted on isolation jars at the motor base served as the electric counterparts to rotary spheres. Energy for the system was supplied by independently charging the base spheres with a hand operated generator. When the two base spheres were placed opposite each other near the rotor perimeter, the rotor began to turn by attractive charge induction until the spheres were close enough for charge transfer by sparking. Then the mutually charged spheres were repelled because of their like charges. This process continued for a half turn bringing the oppositely charged rotor spheres to the opposing base sphere, causing

the motion to accelerate due to the greater charge difference. As the base and rotor spheres aligned, a spark would transfer the base charge to the rotor changing the sphere's polarity. Thus, motion would continue until the isolation jars were discharged.

This type of device demonstrates the principle of electrostatic propulsion but is impractical for application. The torque from this simple case of interaction between oppositely charged spheres is barely sufficient to overcome the axial friction. Thus, the motor could rotate, but none of the mechanical energy could be transferred for external work.

Before the Franklin rotary motor, a reciprocating electrostatic device was built by Andrew Gordon which became know as the "electric bells". Constructed in 1742, it operated by a thin plate swinging rapidly as a pendulum between two metallic cups to produce a ringing sound. The bells were oppositely charged with the plate initially set in motion by induction. When the plate came in contact with one of the bells, charge was transferred to it by conduction. The plate was then repelled by that bell and attracted by the other bell. Motion was then maintained by conduction charge transfer until the charge was dissipated from the bells.

This device designed by Gordon was latter harnessed by Howard B. Daily in 1880 to provide a transition from the oscillatory motion to rotary motion. The machine applied the same principle as the Gordon electric bells with the reciprocating plate attached to a flywheel by a lever arm. The motor was driven in much the same way as a steam engine would drive a locomotive.

As with Franklin's design. the Daily motor operated well against friction but did not provide sufficient torque to be a practical means of energy transfer. Overall. the machines were large and cumbersome with the electric parts being a small portion of the whole system. The concept of the electrostatic motor did not make any significant improvement until the use of interacting charged surfaces was recognized as a means to greatly increase the electric force. Since the use of parallel plates to provide a means of charge storage is called a capacitor. this next level in electrostatic motor design became known as a capacitive motor.

A thorough text on the history of electrostatic motors is provided by Oleg Jefimenko[2]. The illustrations he provides show that most of the basic configurations in study today originated in the eighteen hundreds. Improvements on the early models have been refinements in design as the methods for precision machining and the construction of electric circuit drivers have advanced. There are numerous devices that induce motion by electrostatic means but most of them are more of a novelty than a means of useful energy transfer.

Among the motor design of significance are the works of Karl Zipernowsky. He built two capacitor motors that operated on the principle of synchronous switching of the voltage polarity. The first motor was built in 1889 and had radial electrodes to form a fan-like shape. The second was constructed in 1904 from concentric cylindrical halves. Both possessed the basic characteristic of a capacitor motor which includes a stator and a rotor in a parallel plate arrangement and a means of switching the electric polarity between the

electrodes. Most of the capacitor motors studied in recent decades are of the radial type while the cylindrical model has been investigated as a corona motor.

Fabrication and Circuit Limitations

Precision Machining

Advances in capacitor type motors have followed improvements in fabrication techniques. The motors built before the nineteenth century were made from wood, glass and solid steel spheres. As sheet metal became common in the nineteen hundreds, a series of new designs arose. To increase the motor's operational efficiency, both the design and the method for construction needed changing. Because of the failure of the early electrostatic motors to yield a usable output torque, the electromagnetic type gained wide acceptance as the only electrically activated motor. However, as machining accuracy improved throughout the early twentieth century, the concept of electrostatic motors would resurface as a possible replacement for electromagnetic motors.

The most prevalent design parameter that would determine the victor in the competition between electromagnetic and electrostatic motors is the volumetric energy efficiency. This parameter is a measure of the space occupied by the motor, the motor's weight and the average mechanical energy output compared to the electrical energy input. Electrostatic motors are inherently lighter than electromagnetic motors since the electrostatic design only requires thin conducting surfaces set in thin non-conducting sheets while electromagnetic motors consist of heavy iron magnets and tightly wound coils. Yet,

even with the weight difference, the output from electromagnetic motors was so much greater than electrostatic motors the space and weight factors were irrelevant.

The best hope for the production of a more powerful electrostatic motor was dependent on the modern machining methods to provide extreme accuracy over the interacting surfaces which allowed for the production of precise electrode widths. And since the precision lathing of axle components reduced the wobble as the rotors turned, the gap between the stationary surface and the rotary surface could be narrowed. These milli-inch features increased the motor's performance but left one additional machining problem. To achieve the high precision, the structures had to be thick enough to withstand the machining forces. This requirement added both weight and volume to the motor; so when the mechanical output was greatly increased by the narrow widths, there was still too much metallic bulk to render the motor superior to the electromagnetic type. This problem would not be solved until the 1980s with the introduction microfabrication techniques for machine parts.

The Power Supply

Another consideration for successful operation the electrostatic motors was the power source. The original motors were powered from stored static charge held in bell jars. As batteries and generators became more common, a switching system was devised to provide alternating voltage in a synchronous manner to maintain uniform motion of the rotor. In fact, all capacitor motors require synchronous drivers.

To compensate for the relatively large gap separation between the stator and rotor electrodes, electrostatic motors required a high voltage to generate even a moderate output. Yet as the voltage was increased to provide greater torque, the mechanical switching employed for a uniform drive force caused an additional problem. The increase voltage induced sparking in the switching mechanism which caused the whole system to discharge. Also, the inertia of the switching arm limited its oscillation rate which had to occur quickly for the motor to achieve an appreciable rotary speed.

Thus, a successful electrostatic motor required the development of better fabrication methods for the electrodes and better circuit components for the voltage driver.

Variable Capacitance Motors

The capacitive electrostatic motors have taken on two general configurations. The first type is composed of co-axial stacked disks and the second type employed concentric hollow cylinders. Both possess the advantages of greater interaction area and decreased vertical separation. These two parameters correspond to Coulomb's Law variables with the area of the surface being proportional to the total charge and the separation gap representing the average radial distance between the charges. From this principle, it is clear that the greater the charged surface area and the smaller the gap between the surfaces the greater the electric force. For rotation, the torque would depend on the average radial distance from the axis to the point of average force on the surface. The cylindrical design takes advantage of a maximum radial arm to produce the greatest torque possible whereas the

disk type has a reduced moment arm but is more compact yielding a greater energy output per volume.

The basic design of the capacitive motors, regardless of shape, consists of only a few critical features. First of all, the interacting surfaces are divided into inter-combed electrodes with conducting regions separated by empty space or electrically insulating material. Secondly, the distance between the surfaces must be uniform and as narrow as mechanically possible. Next, the gap between the surfaces can be filled with a liquid dielectric that can also serve as a lubricant. And finally, a synchronous power source is required to supply the alternating voltage that changes polarity to maintain a consistent motion.

Recent Electrostatic Motor Designs

The Macro Motors

One of the first successful cylindrically shaped motors was presented in Russia in 1958. Technically, it was a corona motor since it develops torque by charge induction. The motor itself was considered very efficient but the power source for the motor was not. Normal operation at 6000 rpm required a drive potential of 7000 Volts. The energy lost maintaining the high voltage supply erased any advantage gained from the new motor design.

An extensive description of a variable capacitance disk type motor is presented by B. Bollée in the Phillips Technical Review[3] published in 1969. His designs layout all the characteristics necessary for a reliable electrostatic motor. The electrode pattern for his

motor is like that presented by Zipernowsky except the electrode angle is reduced to provide more interacting regions. He also reduced the stator to rotor gap and stacked them in alternating stages to provide multiple layers. His description of a synchronous voltage driver with the switching mechanism that can deliver a step-wise potential varied between positive, zero and negative is now the standard for radial electrode motor designs. These improvements made by Bollée set the direction for all variable capacitance motors to follow. In spite of his many innovations, the motors were still too bulky and the operational voltage was too high for the efficiency to reach the level necessary to compete with electromagnetic motors.

Among the recently patented electrostatic motors is one presented by J. Staudte [4]. This is actually the same design as the Zipernowsky and the Bollée radial motors but the outer radius is reduced to provide a mechanical driver that can fit inside a common wrist watch. Though very small, the motor is not classified as a micro-scale device. Its dimensions qualify it as miniature. Herein is the distinction between miniature and microscopic. The motor is fabricated using micro lithography methods to produce features with micron precision; however the structure itself has dimensions on the order of centimeters. As a general rule, a true micromotor has a diameter that is less than a millimeter.

Another motor of interest was patented by L. S. Ferriss and R. M. Hohenstein in 1976[5]. The motor body is a conical cross between the radial electrode pattern and the pure cylindrical design. It is intended to be a type of counter rotating gyro that does not deliver

any usable work. The circuit driver maintains the motor's rotational speed against axial friction and the inertial imbalance induced by external motion.

The Micromotors

A true micromotor is defined by its small diameter and the dimensions of its parts. As mentioned above, a miniature motor may be produced using microfabrication techniques to provide features with micron precision yet not have any microstructures as parts. The broad classification of micro actuators includes linear, rotational, vibrational and oscillatory motion. These devices take on various forms and functions such as pumps, valves, turbines, sliders, filters and rotational motors[6].

Practical micromotor design is limited by the available methods of fabrication; thus among the possible designs there are three configurations for producing torque electrostatically. As result of using only lithographic surface machining, which employs sequential layering, two of the designs are inherently weak.

The first is a wobble motor that operates by attracting a central pillar mounted in a cone well to electrode pads around the cone's perimeter. As charge is induced on one of the pads, the pillar leans in its direction. Then the voltage is released from the pad and applied to a neighboring electrode. The pillar then swings toward the newly charged pad. This process continues around the circumference and is repeated to yield rotational motion. Instead of using a wobbling pillar, the second design has a shaft mounted rotor surrounded by electrodes. The outer diameter of the rotor is slightly less than the inner diameter of the electrodes. Since the ends of the rotor are close to the edges of the electrodes, this type of

motor is known as an edge driver. Both the edge drive and the wobble motors turn at appreciable speeds but neither is capable of delivering useful output. This occurs because the area of interaction is only a fraction of the total size of the motor. This limited use of space means the bulk of the motor is not producing useful work. To overcome this problem, the design of the third motor type returns to the variable capacitance arrangement.

In 1987, a group at AT&T published their design of a small flat silicon based micromotor[7] that was then patented in 1988 [8]. This third type has become known as a surface drive motor because it uses the area between the rotor and stator for electrode interaction. Though they call their invention a micromotor, its diameter is on the order of centimeters with electrodes that are only microns wide. Actually it is a miniature motor composed of micro structures on the active surfaces. The AT&T group presented several predictive equations; however the major features of an electrostatic micromotor were described in greater detail by Bart and Lang in 1989[9]. They presented analytical formulas that are intended for the design of the motors on the order of 50 microns in diameter but their formulas and methods are valid on a larger scale also.

To further enhance design development, more accurate formulas were necessary for the prediction of the output force and torque generated by linear and rotary electrostatic actuators. The need for position dependent capacitance values was first recognized by Mahadevan[10] and then later by Kumar and Cho[11]. Knowledge of the capacitance allows direct calculation of the work done by the rotor. Though the calculation methods are tedious, this significant step in analysis is verified by experiment.

Success with a Linear Electrostatic Actuator

A highly successful application of electrostatic propulsion has been presented by a Japanese group which published consecutive articles about their work from 1990 to 1994[12, 13, 14, 15, 16]. Their stacked linear actuator demonstrated the ability of electrostatic force to achieve appreciable work at relatively low voltages. Among all of the electrostatic motors, their invention is possibly the first demonstration of electrostatic propulsion as advantageous over electromagnetic.

The Egawa group also introduced a new material that simplifies the structure of surface driven electrostatic actuators. The special carbon coated polyamide film has a unique property of charge embedment. This is different from electret objects that are permanently polarized. The embedding phenomenon is presumed to arise from a type of interlayer surface resistivity that provides a region which holds the charge temporarily. To activate the film, it is placed in an electric field causing charge to accumulate in the effected region. When the field is removed, the charge slowly dissipates by self-repulsion. The time delay for the dissipation allows the film to behave as an electro-active object. The material appears to be produced by sputtering carbon onto one side of a heat treated film; however, the exact manufacture process is held by Mitsubishi Kasei Corporation of Japan as a trade secret.

Based upon the linear film actuator, a typical rotary design was proposed and studied by analytical, numerical and experimental investigation at Louisiana Tech University[17, 18, 19]. The analytical studies led to the discovery of an optimized design that is the subject of this dissertation.

New Conductors

Recent developments in micromachine processing have occasionally intertwined with research into increasing the quality of conductors. Two major areas of development are cryogenic studies of superconductors and polymer research which has sought to produce conducting plastics. While the prospects for a high temperature superconductor have dwindled, investigation continues in the search for conducting polymers[20]. These polymers can be shaped into thin wires or spread over the surface of a non-conductor to form the thin lines of a printed circuit board. A reliable conducting polymer that has electric properties near that of copper or steel would provide a substitute for metallic wiring. Because the electrostatic motor does not need iron cores like some electromagnetic motors, there is now the possibility of an all plastic electric motor.

The State of the Art

Currently, none of the electrostatic motors has been able to replace electromagnetic motors for any common application. Because of the lower Joule losses predicted by the principle of electrostatic actuation, the electrostatic design has the potential of being more energy efficient than electromagnetic motors. Modern fabrication methods for micromechanical devices open the opportunity for construction of lightweight electrostatic motor boards with high precision electrodes. Optimization of the electrode pattern can now be performed in an effort to obtain the highest possible performance from an electrostatic motor built using the latest in manufacturing methods.

CHAPTER 1

THE ELECTROSTATIC MOTOR DESIGN BASICS

Edge and Surface Drive

The first electrostatic motors built by Benjamin Franklin are classified as the edge drive type. This minimalistic design was a natural consequence of the limited fabrication methods available at the time. Ironically, roughly 240 years later the first true micromotors were of the edge drive type due to the limits of surface micro-machining. The edge drive design takes advantage of the torque principle: the greater the moment arm, the greater the effect of the drive force. For this design, the electrodes are along the outer edge of the rotor and the inner edge of the stator. An example is given in Figure 1 where the left hand illustration represents the edge drive motor. Thus, the electrodes for this type are side-by-side around the motor circumference.

Another design is based on the capacitive principle of surface drive. Though the region that generates the force is not all at the outer circumference like the edge drive type, the additional surface area produces significantly greater force over the full range of its radial length. The contribution of the torque over the electrode length is like the summed effect of a number of concentric edge driver motors with decreasing diameters. The surface design is composed of two identical electrode patterns placed one over the other. The small gap between the surfaces causes the electrodes to behave as capacitors. The application of an electric potential difference between the stator and rotor electrodes causes the

accumulation of charge. By switching the potential polarity, the electrodes tend to realign and thereby produce torque. The right hand side of Figure 1 shows the basic layout of a surface drive motor.

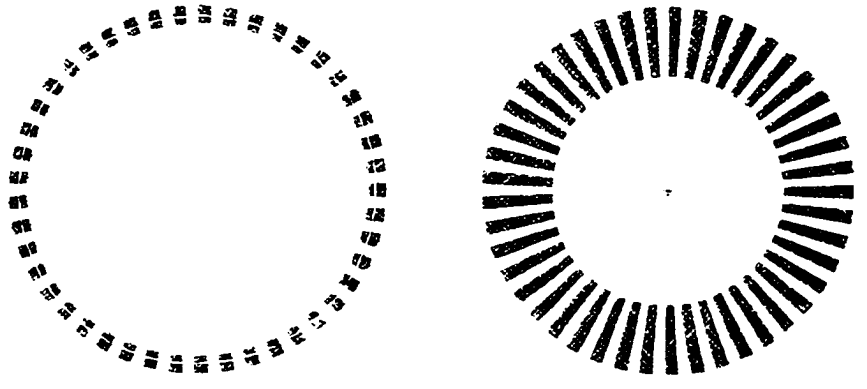

Figure 1 Example of the Edge Drive
and Surface Drive Electrode Patterns

Both of the designs shown in Figure 1 have the same outer diameter and the same number of electrodes. The contrast between the effective charged areas demonstrates the advantage of the surface type over the edge type of drive choices.

Parametric Variations Affecting the Performance of an Electrostatic Motor

The focus for this study is the design of a normal sized electrostatic motor that is constructed with micromachined electrodes. This is the next logical step in the historical design development of electrostatic motors. The previous work that is nearest this goal is that preformed by Gabriel et al [8], Bart and Lang [9] and Egawa et al [12]. The first two worked on the design of rotor motors but failed to quantify the optimum design criteria.

Fabrication Width

The manufacture of micro motors and macro motors with micron sized features is limited by the narrowest structure that can be reliably produced by the fabrication method chosen. As the motor designs have changed through the years, the torque increased as the width of the electrodes decreased. Thus, the first design parameter is fabrication width "s". This value determines the number of electrodes that can fit within a given outer radius.

The Number of Electrode Groups

Both the Gabriel and Egawa groups showed that a three phase switching pattern for the motor's voltage driver provides a means of producing an asymmetric electrode charge arrangement that induces a unidirectional motion. Thus, a group of interacting electrodes includes three conducting regions separated by three insulative regions. As a consequence of the number of electrodes and gaps being six for one electrode group and the radian measure of a full circle being 2π (which is about 6.14), the number of electrode groups (Ng) that can fit around a circle is defined by the ratio of the circle's radius (R) to the fabrication width.

$$Ng \cong \frac{2\pi R}{6s} \cong \frac{R}{s} \qquad (1)$$

Thus, the maximum number of electrode groups that can fit within the outer radius (Ro) of the motor is approximated by Equation 2.

$$N_{g_{max}} = \frac{R_o}{s} \qquad (2)$$

This can be illustrated by considering the case where the fabrication limit is one fifth the outer radius of the proposed motor. The number of possible electrodes patterns is then five. These five patterns are shown in Figure 2.

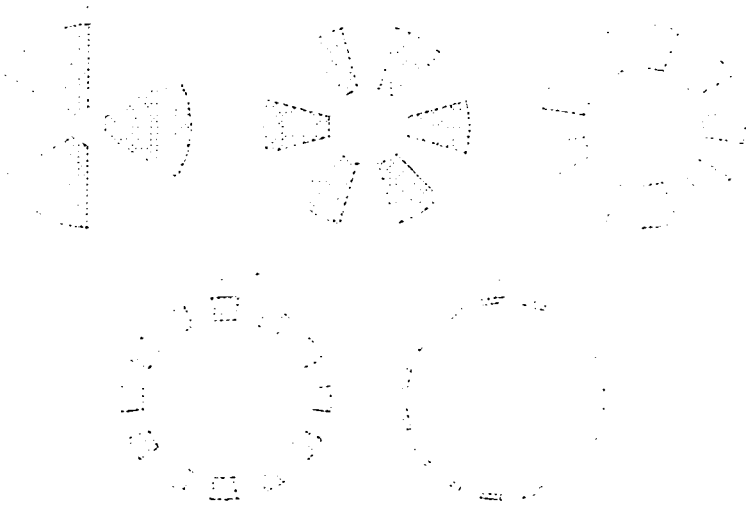

Figure 2 Example of Possible Electrode Patterns

The problem now is to discover which of the possible patterns delivers the greatest torque. One possible method would be to construct all five motor designs and measure the output torque for each. This is simple when the number is small; however, the main application of this electrostatic motor design is actually for cases when the ratio of the outer radius to the fabrication width is large. Thus, a numerical investigation into predicting the output would provide a means of selecting the best motor by simulation rather than experimentation.

Consider the probable effect on the output torque of changing the electrode pattern by generalizing the case given above. For the first case shown in Figure 3, when the number of electrode groups is increased from one to two, the torque is likely to increase because of the small loss in area around the center is compensated by the doubling of the number of interacting electrode pairs.

Figure 3 Transition from the First
to the Second Electrode Pattern

Similarly, when the number of groups is at its maximum value of five, decreasing that number to four reduces the number of interacting pairs by twenty percent but more than doubles the charged area as shown in Figure 4. Thus, the torque should be greater for the case of one less electrode group.

Figure 4 Transition from the Last
to the Previous Electrode Pattern

These two trends are illustrated in the graph shown in Figure 5. Presuming that as the number of electrodes groups increases from the minimum and decreases from the maximum, the torque increases monotonically for both sides, then there is a point where the peak torque is reached. The number of electrode groups that produces the maximum torque determines the best electrode pattern for the given outer radius and electrode fabrication width.

Figure 5 Graphical Representation for Finding the Peak Torque

The Electrode Shape.

The first presumption for the shape of electrodes is the simple radial configuration which is the symmetric division of the circle into equivalent angular parts. But noting that the fabrication limit would only apply to the electrodes around their inner circumference, it is then possible to alter the electrode shape by extending the radial edges until a rectangular gap is reached. Also, the electrode could be narrowed until it is rectangular in shape. For full consideration of the possible effects on the torque, the electrode shape could be any shape that falls between these two extremes. The best shape for the electrodes must be determined simultaneously with the number of electrode groups.

At the first guess, the wider electrode is expected to produce the greater torque because of the increased charge accumulated through the capacitive effect. Another consideration is that as the rotor turns from its initial alignment position to re-align its electrodes with the neighboring stator electrodes, the magnitude of the torque changes due to the reduced Coulomb distance and the change in the projected force vector. However, the overlapping of the electrode tends to reduce the torque between them because the charge is free to move to the electrode edge. Thus, the calculation of the predicted torque must account for both the electrode shape and the variations in the surface charge distribution as the electrodes rotate.

The Stator and Rotor Separation Distance

A fundamental assumption for a capacitive arrangement is that the plate separation distance "z" is much less than its smallest edge dimension. For the parameterization of electrostatic motors, this capacitor characteristic is exchanged for a practical limit on the ratio of the separation distance to the fabrication limit. As the distance "z" is increased compared to the distance "s", the electric field gradient between the stator and rotor electrodes diminishes resulting in a reduced torque. Thus, the separation must not be much greater than the fabrication width. As the distance "z" decreases, both the magnitude of the charge on the surfaces and the resultant angular force between them increases. Clearly, the closer the plates are together in the vertical "z" direction the greater the torque generated between the stator and rotor.

The lower limit on "z" is bound by the fabrication quality of the surfaces. Even when a perfect axle is presumed. the flatness of the surfaces limits "z" both for the stationary case of direct contact and the dynamic case of frictional wear. When the variation in flatness is known for the entire interacting surfaces of the stator and rotor. the separation distance must be at least twice the flatness variation distance plus the size of a lubricant gap that is sufficient to account for axial wobble.

The Controller / Driver

Among the many problems of the early motors is the need for a high drive voltage to account for the large separation gaps. Reducing the electrode size and gaps allows a reduction in the voltage. yet the possibility of arcing must still be considered. The standard method of Paschen curves for the prediction of electrical break-down may be applied provided the scale of investigation and the dielectric material used are the same as those employed for the motor fabrication. Otherwise the motor is expected to behave as a variable capacitor as far as the electrical drive circuit is concerned.

The motor designs presented here are presumed to be three phase as a result of the studies by the Egawa group who showed that uniform electrode spacing and a three step switching scheme produced the most reliable motion. The formulations provide the option of selecting the number of phases by choice the parameter Np. The motor driver is expected to deliver the specified voltage level in a three phase switching pattern at a frequency dependent upon the number of electrode groups and the desired rotation rate. Since the motor must accelerate to the target speed. the drive frequency must be small when the

motor first starts rotating and then increase until the motor reaches its full speed. This may be preformed by monitoring the feedback capacitance which varies in time as the motor rotates. By matching the drive frequency to the feedback capacitance frequency, the motion may be accelerated or maintained at any desired rate.

Rotational Speed and External Load Limits

Under the presumption that a control circuit exists that can deliver a sufficient drive voltage at a wide range of frequencies, there is still an upper limit on the rotational speed due the inertial stress on the thin rotor epoxide base. Though the material is very light-weight, the extremely small thickness necessary for the stack space constraint provides little strength for high speed rotation. The methods for prediction of failure for rotating disks are well established and will not be presented herein; however, calculation of a safe operating limit on the rotation rate should be made for each application of a new motor design.

If the difference between the external load and the drive torque is large enough to cause distortions in the rotor flatness, frictional wear on the electrode coating may occur due to contact between the stator and rotor. A loss in coating thickness can lead to arcing and thus total failure of the drive voltage source. Also, excessive load can lead to slippage of the rotor in its normal motion. This would cause the rotor electrodes to lag behind their predicted position and thus be out of synchronization with the drive frequency.

These two limitations can be programmed into the electronic controller as an upper limit on the drive frequency and as a feedback adjustment to compensate for asynchronous rotation. Thus, the drive circuit is a major part of the successful electrostatic motor.

CHAPTER 2

ACTUATOR PARAMETERS

To provide variables for formulation of the predictive force and torque equations, the dimensions of a linear and a rotary actuator are parameterized based upon representative diagrams. Later, the optimization of the rotary electrode pattern will use a selection of these values with the remaining parameters left as variables to be chosen by the designer. Some of the parameter definitions will apply to both the linear and rotary types and thus will not be repeated in each section.

The two most basic components of an electrostatic actuator are the stator and slider. They are formed from thin flat sheets with a set of electrodes on the two large surfaces. A slider is placed over a stator to form an interacting pair. The double sided stator-slider pairs are stacked to form a propulsion unit. This stack is set in a housing that serves as an outer container and stationary mounting. Under the presumption that the housing unit can be built to any conventional specifications, fabrication of the stator and slider must now be established.

The formation of the electrode pattern on a base board can result from several methods which include the LIGA process of electroforming[21], the silicon process of deposition[22] and the printed circuit board (PCB) process of conductor etching[23, 24]. The choice of the fabrication process determines the minimum feature size of the electrodes and the overall thickness of the stator and slider boards. It also sets the cost of the product.

Using any of these processes, the stator and slider can be made from thin non-conducting wafers with ultra-thin conducting electrodes adhered to the surface. The electrode patterns for both parts are identical. The difference between the two structures is that the stator base board is mounted to the housing, while the slider board is fastened to the movable end mount. Both parts have the same thickness and coating for the electrodes.

Each of the fundamental characteristics of a linear actuator apply to a rotational actuator. The exceptions are that the slider is called a rotor and the rotational output is transferred by a central shaft instead of an end mount.

Beneath each figure with the descriptions given below is a list of the parameters and a brief verbal definition intended to complement the visual representation. As much as possible, standard notation for known variables is used throughout the parameter assignments with the names and symbols forming a mixture of mechanical engineering and electromagnetic theory terms.

The Linear Actuator

The linear actuator has all of the standard features of an electrostatic motor. The simplicity of its electrode pattern will serve as a comparison for the optimization of the rotary pattern. The actuator has a range of motion that is usually limited to about three fourths its body length. Unlike the rotary motor which can turn in one direction indefinitely, the linear type is restricted to an oscillatory motion within its slider's range. Thus, a steady state motion for a linear actuator is not possible.

The Actuator Housing

A linear actuator consists of a housing unit which acts as the stator. The housing is attached to the stationary base with the slider positioned to deliver a fixed range of motion. The device shown in Figure 6 represents a typical linear actuator.

Figure 6 Outer View of a Linear Actuator

Lh: housing length

Wh: housing width

Hh: housing height

With the interior parts removed, the housing provides a cavity for the electrostatic propulsion unit. The dimensions of the interior are reduced from the exterior values by the shell thickness. These dimensions are shown in Figure 7.

Figure 7 Propulsion Unit Dimensions

Lp: propulsion unit length

Wp: propulsion unit width

Hp: propulsion unit height

The Stator and Slider

The top view of a slider board is shown in Figure 8 without the electrode pattern. A stator board is similar with finer mounting holes to attach to the stator end piece. The boards are stacked alternately to provide opposing interaction surfaces.

Figure 8 A Single Slider Board

A cross-section side view of the end mounts shows the alternating stack arrangement of the boards. The stator boards are attached to the right end mount shown in Figure 9 which is fastened to the stator. The left end mount is attached to all the slider boards and serves as the means of force transfer.

Figure 9 Slider and Stator End Mounts

Both the stator and slider boards are composed of three layers. The central layer is the epoxide base board. It provide the mechanical strength and the electrical isolation for the electrodes. A thin copper layer coats both sides of the board. The electrode pattern is a result of photo-etching the copper layers.

The electrodes are formed on both sides of the epoxide base to minimize the stack thickness. The electrodes and base are totally covered by the dielectric coating. Its thickness is defined as the distance from the base board to its surface. Figure 10, which is not to scale, is a cross-sectional view of the board showing the structures with their defined thicknesses.

Figure 10 Cross-Section of a Base Board

Td: dielectric coating total thickness

Tb: epoxide base board thickness

Tc: conductor thickness (Td > Tc)

The total thickness of a stator or slider is given by Equation 3. This parameter is used in the stack calculation to find the total number of boards that will fill the motor housing cavity.

$$T = T_b + 2T_d \tag{3}$$

T: total thickness of a single rotor or stator

The Propulsion Stack

The basic actuator unit consists of a single stator and slider with electrodes on one side. To multiply the effect of a single unit, the flat stators and rotors are produced with electrodes on both sides and then stacked to form a bulk motor. Since the board thickness and the gap between the stator and slider are fixed values, the total height of the stack depends on the number of stator-slider pairs that can fit within the housing cavity.

Figure 11 illustrates a typical stack configuration. This diagram is also not to scale. The aspect ratio of the boards is usually much greater and the gaps are much narrower than the board thickness. The rectangles shifted to the left represent the sliders and the ones shifted to the right represent the stators.

Figure 11 Stack of Stators and Sliders

g: gap distance between stator and slider

The thickness of the whole stack is given by Equation 4. Since the cavity height is a fixed parameter. Equations 4 and 5 are solved to find the number of stators and sliders within the stack.

$$H_p = N_s T + N_{sl} T + 2(N_{sl})g \quad \textbf{(4)}$$

$$N_{sl} = N_s - 1 \quad \textbf{(5)}$$

Ns: number of stators in the stack

Nsl: number of sliders in the stack

For calculation of the Coulomb force, the distance between a stator electrode and a slider electrode is defined as the parameter "z". This value can be found using the board thickness and gap parameters as given by Equation 6.

$$z=2(T_d-T_c)+g \tag{6}$$

z: vertical distance between electrodes in a stator-slider pair

The dielectric coating for the electrodes and the lubricant that fills the gap between the stator and slider possess the physical property of electric permittivity. The magnitude of these values affects the electric force between the electrodes. When a stator and slider are stacked together. the materials yield a triple layered effect which acts as a single material with a composite permittivity expressed by Equation 7.

$$\varepsilon_z=\frac{z}{\frac{g}{\varepsilon_g}+\frac{2(t_d-t_c)}{\varepsilon_d}} \tag{7}$$

εd: permittivity of the dielectric coating

εg: permittivity of the gap material

εz: equivalent permittivity for the layered materials

This calculated value for the permittivity is used in the electrostatic force calculations as the equivalent value for the three layers. In all applications. the dielectric permittivity is the same for both the stator and slider. The gap material is typically a liquid that must be non-conductive and have a high electric strength.

The Electrode Pattern

A single interaction group is composed of three electrodes. This pattern is repeated for the full length of the stator board. The total number of electrode groups that can fit on a base board can be found by rearranging Equation 8.

Figure 12 An Electrode Group

Le: electrode length

We: electrode width

Wg : gap width

$$L_p = N_g(3W_e + 3W_g) \quad \textbf{(8)}$$

The electrode length and the length of the propulsion unit are set by the outer dimensions of the actuator. The electrode width and gap are determined by the fabrication process.

The Rotary Actuator

Since the goal is to produce an electrostatically driven motor that could replace the electromagnetic type, the electrostatic propulsion components should be able to fit within the housing of an electromagnetic motor available commercially. Thus, the description for the rotary motor begins with a conventional motor housing.

The Motor Housing

The outer view of an electromagnetic motor provides the target dimensions for the design of an electrostatic motor. Figure 13 shows the outer dimensions of the housing length and diameter.

Figure 13 Outer View of an Electromagnetic Motor

Lh: total length of the housing

Dh: outer diameter of the housing

The housing cavity provides the space constraint for the propulsion unit that forms the drive components of an electrostatic motor. A shell thickness for the housing is

presumed to be sufficient to provide the structural strength necessary for a viable motor. With the end pieces and the electromagnetic components removed, the main cylinder of the housing provides a cavity for the electrostatic components. The cylinder is shown in Figure 14 with notches drawn in anticipation of the stator board design.

Figure 14 Dimensions for Motor Cavity

Lp: propulsion unit length

Dp: propulsion unit diameter

The Stator, Rotor, and Shaft

An overview of the stator and rotor base boards is shown in Figure 15. The electrode pattern will be explained later. The stator must fill the cavity and have a means of securing itself against rotation. Likewise, the rotor inner diameter has a means for connection to the shaft. The rotor's outer diameter is less than the stator's to allow space for rotation and the stator's inner diameter is greater than the rotor's to allow for shaft rotation. The shaft is formed from a compression molded structure that fills the rotor cavity and a central metallic rod for delivering the torque externally as is conventional.

Figure 15 The Stator and Rotor Boards

Dso: stator outer diameter

Dsi: stator inner diameter

Dro: rotor outer diameter

Dri: rotor inner diameter

Figure 16 The Rotor Shaft

The Propulsion Stack

Stacking the stator-rotor pairs follows the same convention as described above for the linear actuator. In Figure 17, the larger rectangles represent the stators and the smaller ones represent the rotors.

Figure 17 The Propulsion Stack

The thickness of the whole stack is given by Equation 9. The distance includes a gap that is added to both ends for clearance with the housing.

$$L_p = N_s T + N_r T + 2(N_s + 1)g \quad \textbf{(9)}$$

$$N_r = N_s + 1 \quad \textbf{(10)}$$

Ns: number of stators in stack

Nr: number of rotors in stack

The Electrode Pattern

The electrode pattern must fit between the outer diameter of the rotor and the inner diameter of the stator. For illustration here only, Figure 18 shows a disk drawn with those dimensions as a representation of a stator or rotor to assist in the pattern definitions. Figure 19 shows a group of radial electrodes as an example to establish the basic electrode variables. The electrode's width can vary as defined by the shape angle.

Figure 18 The Electrode Base **Figure 19** An Electrode Group

Ro: electrode pattern outer radius (Dro > 2 Ro)

Ri: electrode pattern inner radius (2 Ri > Dsi)

θ: electrode angle

s: smallest feature size

The value of "s" is fixed so that as the inner radius takes on any value less than the outer radius, the electrode angle changes according to Equation 11.

$$\theta = 2ArcSin(\frac{s}{2R_i}) \qquad (11)$$

For every electrode there is a gap so that the total number of electrodes that fill the circular pattern is half the proportion of θ to 2π.

$$N_e = \frac{\pi}{\theta} \tag{12}$$

Ne: number of electrodes

The motor is driven by an electronic circuit that switches the voltage among the electrodes in a three phase sequence. For this reason it takes three electrodes to form a group. The choice of the number of electrode groups is the main focus of the optimization process.

$$N_g = N_p N_e \tag{13}$$

Np: number of switching phases (Np=3)

Ng: number of electrode groups

The Electrode Shape

As an example for Figure 19, the electrodes are illustrated as having a radial shape. Actually, the electrodes can have any of the three shapes shown in Figure 20 or any variation in between. The shapes can be quantified by the parameter α which can be any value from zero to θ. An α greater then θ will reduce the gap between electrodes below the value of s which is the fabrication limit.

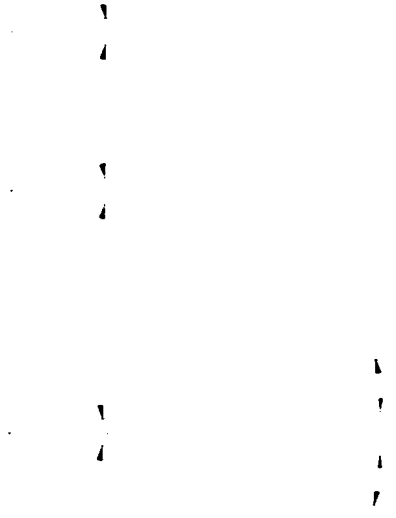

Figure 20 The Electrode Shapes

α: electrode shape angle

Unlike the electrode angle that is measured from the center, the shape angle pivots at the inner edge of the electrode. Though the angle α is only shown in the last illustration in Figure 8, all the electrode shapes can be described by α as given in the table below.

Table 1 Defined Shape Angles

Electrode Shape	α	Gap Shape
Rectangular	0	Wedge
Radial	θ/2	Radial
Wedge	θ	Rectangular

Parameter Lists

A summary listing of the linear and rotary parameters is provided for convenient reference. The parameters needed for each actuator type are listed independently in each table. The parametric relations important to the optimization process are compiled in Table 3. Note that only four of the parameters are needed for optimization of the electrode pattern.

Table 2 Linear Parameter Summary

Lh	housing length
Wh	housing width
Hh	housing height
Lp	propulsion unit length
Wp	propulsion unit diameter
Hp	propulsion unit height
Td	dielectric coating total thickness
Tb	epoxide base board thickness
Tc	conductor thickness
T	total thickness of a single rotor or stator
g	gap distance between rotor and stator
Ns	number of stators in the stack
Nsl	number of sliders in thestack
z	vertical distance between electrodes in a stator-rotor pair
εd	permittivity of the dielectric coating
εg	permittivity of the gap material
εz	equivalent permittivity for the layered materials
Le	electrode length
We	electrode width
Wg	gap width

Table 3 Summary of Rotary Parametric Relations

The outer dimensions of the housing determines: Ro, Ns and Nr
The electrode fabrication process sets the value of s, εd and εg.
The optimization process requires the fixed values of Ro, s, z and εz.
The optimum process returns the values of Ng, and α .
The value of Ng sets the values of θ and Ri which determine the electrode pattern.

Table 4 Rotary Parameter Summary

Lh	total length of the housing
Dh	outer diameter of the housing
Lp	propulsion unit length
Dp	propulsion unit diameter
Dso	stator outer diameter
Dsi	stator inner diameter
Dro	rotor outer diameter
Dri	rotor inner diameter
Td	dielectric coating total thickness
Tb	epoxide base board thickness
Tc	conductor thickness
T	total thickness of a single rotor or stator
g	gap distance between rotor and stator
Ns	number of stators in stack
Nr	number of rotors in stack
z	vertical distance between electrodes in a stator-rotor pair
εd	permittivity of the dielectric coating
εg	permittivity of the gap material
εz	equivalent permittivity for the layered materials
Ro	electrode pattern outer radius
Ri	electrode pattern inner radius
θ	electrode angle
s	smallest feature size
Ne	number of electrodes
Np	number of switching phases
Ng	number of electrode groups
α	electrode shape angle

CHAPTER 3

THE MOTION EQUATIONS

Formulation of the Linear Models

The model for calculating the drive force can be reduced to the interaction of one electrode on the stator with one electrode on the slider. Under the assumption that the electrode charge can be predicted using the basic capacitance equation, the displacement force is estimated as the Coulomb attraction between the offset electrode pair. Once this force formula is known, the total force is then the summation of this term for all the stator and slider electrodes.

The Line Integral Method

For the first estimate of the force between electrodes, the surface charge distribution is reduced to a constant line charge for simplicity. This allows direct integration into a closed form solution. The method begins with the definition of capacitance which is written as:

$$q = CV \tag{14}$$

With capacitance relation for a parallel plate capacitor given as:

$$C = \frac{\varepsilon A}{z} \tag{15}$$

with the spatial terms defined in Figure 21. Here, ε is the electric permittivity of the material between the plates.

Figure 21 Capacitance Parameters

Equation 15 is written under the presumption that the dimensions for the surface areas of the two identical plates are much greater than their vertical separation. For all the actuators under study, the electrode width is on the same order of dimension as their separation. As a result of this spatial feature, the electric field is not uniform but rather behaves more like a dipole. Thus, this equation can give only a first estimate of the charge characteristics of the electrode interactions.

To reduce the Gaussian based force expression to a double integral, the width of the electrode can be disregarded leaving only a linear charge distribution which is defined as:

$$\lambda = \frac{q}{L} \tag{16}$$

Combining these equations with the area expressed as the product of the length and the width, the linear charge density of each electrode can be written as:

$$\lambda = \frac{\varepsilon w V}{z} \tag{17}$$

With this definition, Gauss's Law for the element of lateral propulsive force between two interacting electrodes can be formulated as:

$$dF_x = \frac{dq dq'}{4\pi\varepsilon r^2} Sin(\phi) \tag{18}$$

Figure 22 shows all the terms for a surface charge calculation. To obtain the variables for the line integration, the width is ignored and the line of charge is taken to lie along the electrode's center.

Figure 22 Linear Model Variables

The direct distance between charge elements is found to be Pythagorean.

$$r^2 = (l - l')^2 + z^2 + x^2 \tag{19}$$

And the projection angle that yields the force component in the direction of drive is written as:

$$Sin(\phi)=\frac{x}{[(l-l')^2+z^2+x^2]^{1/2}} \tag{20}$$

Combining Equations 18, 19 and 20 gives the complete integration as:

$$F_x=\frac{\lambda^2}{4\pi\varepsilon}x\int_0^L\int_0^{L'}\frac{dldl'}{((l-l')^2+z^2+x^2)^{3/2}} \tag{21}$$

which with L and L' being equal results in empirical expression:

$$F_x=\frac{\lambda^2x(\sqrt{L^2/(x^2+z^2)+1}-1)}{2\pi\varepsilon\sqrt{x^2+z^2}} \tag{22}$$

Substitution the Equation 17 for the linear charge density gives the final expression for the drive force.

$$F_x=\frac{\varepsilon xw^2V^2(\sqrt{L^2/(x^2+z^2)+1}-1)}{2\pi z^2\sqrt{x^2+z^2}} \tag{23}$$

This shows that the force depends on several factors that are true for all electrostatically driven actuators. First, the force is directly proportional to the magnitude of the permittivity and to the square of the applied voltage difference. Secondly, as the length of the electrodes is increased, the force increases. And finally, the smaller the gap distance "z" the greater the force.

One of the major flaws to this type of derivation is that the reduction of the charge distribution to the linear form causes this equation to give false relations of increased force with increased electrode width. Actually, due to the overlap phenomenon, which will be discussed later, the force decreases as the electrodes become aligned. Likewise, the vertical force component can be formulated and expressed as follows:

$$F_y = \frac{\lambda^2}{4\pi\varepsilon} z \int_0^L \int_0^L \frac{dl dl'}{((l-l')^2+z^2+x^2)^{3/2}} \tag{24}$$

which yields:

$$F_y = \frac{\lambda^2 z(\sqrt{L^2/(x^2+z^2)+1}-1)}{2\pi\varepsilon\sqrt{x^2+z^2}} \tag{25}$$

and in its final form gives:

$$F_y = \frac{\varepsilon w^2 V^2(\sqrt{L^2/(x^2+z^2)+1}-1)}{2\pi z\sqrt{x^2+z^2}} \tag{26}$$

The Surface Integral Method

The force integral can be extended to include the width of the electrodes with the surface charge distribution given by the unknown function σ.

$$F_x = \int_0^L \int_0^L \int_{-\frac{w}{2}}^{\frac{w}{2}} \int_{-\frac{w}{2}}^{\frac{w}{2}} \frac{\sigma\sigma'(x-w+w')dwdw'dldl'}{4\pi\varepsilon((l-l')^2+z^2+(x-w+w')^2)^{3/2}} \tag{27}$$

$$F_y = \int_0^L \int_0^L \int_{-\frac{w}{2}}^{\frac{w}{2}} \int_{-\frac{w}{2}}^{\frac{w}{2}} \frac{\sigma\sigma' z dw dw' dl dl'}{4\pi\varepsilon((l-l')^2+z^2+(x-w+w')^2)^{3/2}} \quad (28)$$

The charge distribution depends on the relative location of the electrodes and thus is a function of "x". Without knowledge of the surface charge densities, the above equations can not be integrated directly. This problem has been recognized by others who proposed solutions by finding the capacitance of the electrode system. Among these are Mahadevan[10] whose numerical results are compared with experimental data to verify the predicted trend. Later, Kumar and Cho[11] used a perturbation method which more accurately predicted both the capacitance and charge density.

Formulation of the Rotary Models

The Line Integral Method

Using the same premise as the linear model given above, with the exception that the line charges are coplanar, an expression for the torque can be written as

$$\tau = \int \tilde{r} \times d\tilde{F} \quad (29)$$

with the element of perpendicular force expressed as:

$$dF_{\perp} = \frac{dq dq'}{4\pi\varepsilon(r^2+r'^2-2rr'Cos(2\theta))} Sin(\phi) \quad (30)$$

the torque integral takes on the form:

$$\tau = \frac{\lambda^2}{4\pi\varepsilon}\int_{Ri}^{Ro}\int_{Ri}^{Ro}\frac{rr'\sin(2\theta)}{(r^2+r'^2-2rr'Cos(2\theta))^{3/2}}drdr' \qquad (31)$$

The spatial variables are defined in Figure 23. The 2θ term is used because the electrodes have an angular width of θ and thus their angular separation between electrode centers is twice that value.

Figure 23 The Line Charge Variables

Integration gives the result:

$$\tau = \frac{\lambda^2[(Ro^2+Ri^2-2RoRiCos(2\theta))^{1/2}-(Ro+Ri)Sin(\theta)]}{2\pi\varepsilon Sin(2\theta)} \qquad (32)$$

The linear charge distribution is now re-derived with the length expressed as the difference between the radii;

$$L = R_o - R_i \qquad (33)$$

and the electrode area (Equation 34) is then the angular portion of the ring formed by the radii as shown in Figure 24.

$$A=\theta(R_o^2-R_i^2) \tag{34}$$

Figure 24 Radial Variables

With the area given by Equation 34 substituted into Equation 15 and the length given by Equation 33 used in Equation 16, the expression for λ is transformed for the radial case to yield

$$\lambda=\frac{\varepsilon\theta(R_o^2-R_i^2)V}{d(R_o-R_i)} \tag{35}$$

The final expression for torque is then:

$$\tau=\frac{\varepsilon\theta^2(R_o^2-R_i^2)^2V^2[(Ro^2+Ri^2-2RoRiCos(2\theta))^{1/2}-(Ro+Ri)Sin(\theta)]}{2\pi d^2(R_o-R_i)^2Sin(2\theta)} \tag{36}$$

The coplanar radial model assumes infinitely thin lines of charge and thus the angle can be infinitely small and yield the same form of the predicted torque. Though numerically possible, this is not true physically since the torque goes to zero as the electrodes align. Thus, this model may be used to predict center line torques at the initial position only.

The Surface Integral Method

The torque equation can be written more accurately by including the surface charge distribution for each electrode. A convenient means of derivation is to first write the potential energy for the arrangement then find the torque by differentiation. Starting with the energy form of Gauss's law expressed as integration elements in Equation 24. the element of electric potential energy is:

$$dU = \frac{dqdq'}{4\pi\varepsilon R} \tag{37}$$

with the spatial terms shown in Figure 25.

Figure 25 Surface Integral Spatial Variables

The charge elements are defined by the radial area terms and the surface charge density.

$$dq = \sigma dr(rd\theta) \tag{38}$$

The area elements are shown in Figure 26.

Figure 26 Integration Element Variables

The charge distribution terms can be incorporated to yield

$$dU = \frac{[\sigma dr(rd\theta)][\sigma' dr'(r'd\theta')]}{4\pi\varepsilon(r^2 + r'^2 - 2rr'Cos(\psi - \theta + \theta') + z^2)^{1/2}} \qquad \textbf{(39)}$$

For the general case investigated here, the electrode shape is not considered to be strictly radial. To account for possible variations on the electrode area, a shape angle is introduced which allows for examination of all practical electrode shapes that can be produced by varying the electrode shape from a rectangle to an extended wedge as shown in Figure 27.

Figure 27 Wedge Shaped Electrode

This changes the integral limit from θ to a function of the radial integration variable θr.

Here, ϕ is an integration form of the design parameter α. It ranges from a minimum value for a rectangular shaped electrode when α is zero to a maximum value for a wedge shape when α equal θ.

$$\phi_{min} = ArcSin(\frac{s}{2R_o}) \tag{41}$$

$$\phi_{max} = \theta - \phi_{min} \tag{42}$$

The upper limit on ϕ is a result of the fabrication parameter for minimum feature size defined as "s".

Combination of the above expressions yields the full surface integral for the potential energy of two interacting electrodes as

$$U = \int_{R_i}^{R_o}\int_{R_i}^{R_o}\int_{-\theta_r}^{\theta_r}\int_{-\theta_r}^{\theta_r} \frac{\sigma\sigma' rr'}{4\pi\varepsilon(r^2 + r'^2 - 2rr'Cos(\psi - \theta + \theta') + d^2)^{1/2}} d\theta d\theta' dr dr' \tag{43}$$

The torque acting between the electrodes is then found by the expression

$$\tau = \frac{\partial U}{\partial \psi} \tag{44}$$

which yields

$$\tau = \int_{R_i}^{R_o}\int_{R_i}^{R_o}\int_{-\theta_r}^{\theta_r}\int_{-\theta_r}^{\theta_r} \frac{\sigma\sigma' r^2 r'^2 Sin(\psi - \theta + \theta')}{4\pi\varepsilon(r^2 + r'^2 - 2rr'Cos(\psi - \theta + \theta') + z^2)^{3/2}} d\theta d\theta' dr dr' \tag{45}$$

as the overall equation for torque. The total torque acting on the rotor is the sum of all the stator and electrode group interactions. This can be expressed as

$$\tau_{rotor} = N_g \tau_g \tag{46}$$

The torque generated by an electrode group can be approximated as the sum of the effects within the group as interacting with the opposing stator's electrode group and its two neighboring groups. If the above torque integral is written in a simplified form which includes only the positional variable

$$\tau = \tau(\Psi) \tag{47}$$

then the group torque can be expressed as an extended sum which includes interaction with the aligned stator group, the forward group and the rear group.

$$\tau_g = \tau_{g_A} + \tau_{g_F} + \tau_{g_R} \tag{48}$$

A charge pattern from Egawa[12] is shown in Figure 28 with the angle dependent torque equations formed by considering the interaction of the positive rotor electrode with each stator electrode in a group, then following the same scheme for the negative rotor electrode and repeating the process for all three groups. Since the electrode centers are separated by an angle of 2θ, the position angle is always offset by a multiple of that value.

Figure 28 Representation of Charged Electrode Groups

The sum may be compiled by considering the pattern for the first case. Using the notation of "R" for rotor and "S" for stator with the subscripts representing the positive and negative polarities. the interaction between electrodes can be written in a pseudo-equation such as Equation 49.

$$\tau_{g_A}=[(R_{-}\text{-}S_{-_A})+(R_{-}\text{-}S_{-_A})]+[(R_{-}\text{-}S_{-_A})+(R_{-}\text{-}S_{-_A})] \quad \textbf{(49)}$$

From this the change in the angular position variable can be written considering that motion is indicated by Ψ increasing from zero to 2θ. Thus. Equation 48 can be translated into Equation 49 to yield Equation 50.

$$\tau_{g_A}=[\tau(\Psi)+\tau(2\theta-\Psi)]+[\tau(\Psi)-\tau(4\theta-\Psi)] \quad \textbf{(50)}$$

Likewise. the two remaining group equations can be found as follows

$$\tau_{g_F}=[\tau(8\theta-\Psi)-\tau(6\theta-\Psi)]+[\tau(8\theta-\Psi)-\tau(10\theta-\Psi)] \quad \textbf{(52)}$$

$$\tau_{g_R}=[\tau(\Psi+6\theta)-\tau(\Psi+4\theta)]+[\tau(\Psi+2\theta)-\tau(\Psi+4\theta)] \quad \textbf{(51)}$$

Each of the torque functions requires integration over the two interacting surfaces. When a closed form solution for the general integral is not known. the only alternative is numerical integration. The total process of calculating all the surface charge distributions and then calculating the integrals is extremely difficult even with advanced computing methods.

An Alternative Form of the Electric Potential

This method of extensive calculation can be circumvented by recognizing that the energy equation can be rewritten as the product of the charge on one of the electrode surfaces and the potential at that surface is due to the other electrode. That is.

$$U = q\Phi = \int \Phi dq = \int_{R_i}^{R_o} \int_{-\theta_r}^{\theta_r} \Phi(r)\sigma' r' dr' d\theta' \tag{53}$$

with the charge element being the same as Equation 38 and the potential at that charge element due to the other electrodes being

$$\Phi(r) = \int_{R_i}^{R_o} \int_{-\theta_r}^{\theta_r} \frac{\sigma}{4\pi\varepsilon(r^2 + r'^2 - 2rr' Cos(\psi - \theta + \theta') + z^2)^{1/2}} r d\theta dr \tag{54}$$

However. this formula for the electric potential is the same expression for the potential based on Green's function which has the form

$$\phi(\tilde{r}) = \frac{1}{4\pi\varepsilon} \int_{S'} \frac{1}{|\tilde{r} - \tilde{r}'|} \sigma(\tilde{r}') d\tilde{s}' \tag{55}$$

Thus. the numerical method of boundary elements. which is derived from the Green's functional form of the electric potential, may be applied to find both the energy and the torque resulting from the electrostatic interaction of the stator and rotor electrodes.

The General Torque Equation

The electrostatic motor is composed of regions of constant electric potential that interact to produce torque. The charged regions are spatially symmetric in shape but asymmetric in polarity. The stator and rotor electrode patterns are identical with the relative position of the oppositely charged regions offset by rotation to yield a field gradient which induces the torque. Due to the constant nature of the impressed voltage, the system is governed by electric potential theory. Derivation of a torque equation for prediction of the motive response is given below.

The electric potential is governed by the Laplace equation.

$$\nabla^2\Phi = 0 \tag{56}$$

A solution to this equation with the electrodes providing the boundary conditions as surfaces of constant potential would have a functional form of

$$\Phi = \Phi(r, \theta, z) \tag{57}$$

When this empirical function is known for all space, the rotor torque can be calculated based on its derivatives. To develop that relation, we must first begin by resolving the overall torque into its elements. Thus, the total torque on the rotor is the sum of the torques generated for each rotor electrode group.

$$\tau_{rotor} = \sum_{g=1}^{N_g} \tau_g \tag{58}$$

The torque within an electrode group is the sum of the torques on the three electrodes each of which has a potential that is positive, negative or zero.

$$\tau_g = \tau_{e_r} + \tau_{e_\theta} + \tau_{e_0} \tag{59}$$

Each of these values is found by integration of the electric force over the electrode's surface.

$$\tau_e = \int_S \tilde{r} \times d\tilde{F} \tag{60}$$

The element of angular force is a result of the presence of charge in the local electric field with the charge element expressed as the free surface charge density within a surface element.

$$dF_\theta = E_\theta dq = E_\theta(\sigma_f ds) \tag{61}$$

The free surface charge density is equivalent to the normal component of the electric field in the local medium which for this case is the Z direction because the electrode regions are all parallel to the X-Y plane.

$$\sigma_f = \varepsilon E_z \tag{62}$$

By definition, the electric field is the gradient of the electric potential.

$$\tilde{E} = -\tilde{\nabla}\Phi \tag{63}$$

So, the rotational component of the electric field is:

$$E_\theta = -\frac{\partial \Phi}{\partial \theta} \tag{64}$$

and the surface charge density can be expressed as

$$\sigma_f = -\varepsilon \frac{\partial \Phi}{\partial z} \tag{65}$$

This allows the elemental force to be rewritten as:

$$dF_{\theta} = \frac{\partial \Phi}{\partial \theta} \varepsilon \frac{\partial \Phi}{\partial z} ds \tag{66}$$

and since the radial arm and the force are now perpendicular, the cross product becomes a scalar multiple reducing the torque integral to

$$\tau_e = \int_S \varepsilon r \frac{\partial \Phi}{\partial \theta} \frac{\partial \Phi}{\partial z} ds \tag{67}$$

Finally, this equation shows that the rotor torque can be expressed in terms of spatial operations on the electric potential in the dielectric medium quantified by the permittivity constant. Absence of an empirical expression for the scalar function leads to the application of numerical methods.

The Boundary Element Method

The preferred numerical method for field calculations is the boundary element method (BEM). By considering elements only on the electrically active boundaries, the electric potential can be determined at any point in space. This potential is easily represented in integral form when the surface distribution of charge at the source is known. For the case of a constant potential, the Dirichlet boundary condition applies which allows the potential function to be written as:

$$\phi(\vec{r}) = \frac{1}{4\pi\varepsilon}\int_{S'} G(\vec{r},\vec{r}')\sigma(\vec{r}')d\vec{s}' \tag{68}$$

where G is Green's function.

$$G(\vec{r},\vec{r}') = \frac{1}{|\vec{r}-\vec{r}'|} \tag{69}$$

Also, the condition for continuity must be applied at every boundary surface.

$$(\varepsilon_1 - \varepsilon_2)\int_{S'} G(\vec{r},\vec{r}')\sigma(\vec{r}')d\vec{s}' + (\varepsilon_1 + \varepsilon_2)\sigma(\vec{r}) = 0 \tag{70}$$

The further derivation of boundary element technique applies the method of weighted residuals to find an equivalent source that yields the same potential as the applied boundary constraints and satisfies the continuity condition[25, 26, 27]. Thus, the surface charge density distribution is approximated to yield the constant potential on the electrode surfaces, then that charge distribution is integrated to find the electric potential at the desired points. This can be express parametrically by signifying each spatial surface element with the index "i" and accumulating a matrix of potentials with their derivatives. Thus, the boundary element method finds for each i:

$$\Phi_{r_i}, \Phi_{\theta_i}, \Phi_{z_i} \tag{71}$$

and

$$\frac{\partial\Phi_i}{\partial r}, \frac{\partial\Phi_i}{\partial\theta}, \frac{\partial\Phi_i}{\partial z} \tag{72}$$

For the specific case of the torque calculation, the potential gradients in the angular and vertical directions are found at each of the rotor electrode's elements. The radial arm from the specified axis to each element is factored into the integral which is compiled as a sum of all the elemental effects.

$$\tau_e = \sum_i r_i \varepsilon_i \frac{\partial \Phi_i}{\partial \theta} \frac{\partial \Phi_i}{\partial z} A_i \qquad (73)$$

Here, "A_i" is the area of the element and "ε_i" is the permittivity of the material on the field side of that area.

This method has been implemented in computer code by Integrated Engineering Software, Inc[28]. The application of the boundary element method for electrostatics is contained in their program titled COULOMB. The numerical data for the optimization process were obtained by modeling the electrostatic motor electrode pattern with the graphics editor and running the program to obtain the predicted torque output directly.

Analysis of the AT&T Motor

The AT&T motor design is based on alignment criteria [8] by starting with the smallest imaginable electrode widths and increasing the size until a suitable stability is reached. They do not provide a method for determining a preferred electrode pattern.

There are two major design flaws that should be noted. The first is that the ultra small line width advantage of silicon technology allows the production of electrodes that are only six microns wide. For the electrostatic drive to work effectively, the vertical gap between the stator and rotor must be less than the electrode width. They use a one micron gap to meet this condition, but this is much too small for any fabrication process to yield

a flatness that will keep the gap consistent during rotation. The other flaw is that their design for both the linear and rotary actuator use the rectangular electrode shape. The preferred electrode shape for a circular pattern is radial. Thus, the highest possible torque their design can generate is reduced below the optimum based on the electrode shape alone.

The torque equation for estimation of output of the their motor [7] was derived beginning with the relation for the capacitance of two parallel rectangular plates of width "w", length "l", separation "d" and filled with a dielectric of permittivity "ε".

$$C=\frac{\epsilon w l}{d} \tag{74}$$

For the next step they wrote the electric potential energy using the definition based on a parallel plate capacitor.

$$U=\frac{1}{2}CV^2 \tag{75}$$

The propulsive force equation is found by taking the partial derivative of the energy equation in the direction of motion. Since the motion of the actuator is across the width of the electrodes, the derivative eliminates the "w" term.

$$F_x=-\frac{\partial U}{\partial x}=-\frac{1}{2}\frac{\epsilon l V^2}{d} \tag{76}$$

By translation of the length term into the corresponding radial increment, the force is integrated over the length of the electrode to give the expression for the collective interaction of all charged electrodes as:

$$\tau = \int_{Ri}^{Ro} \frac{\pi \epsilon V^2}{dnp} r^2 dr \tag{77}$$

which yields the solution of

$$\tau = \frac{\pi \epsilon V^2}{3dnp} [Ro^3 - Ri^3] \tag{78}$$

Where "n" is the number of phases and "p" is the linear pitch between electrode centers which is always twice the electrode width. All of the other parameters are the same as described for the other models.

The optimization process requires the variation of the number of electrodes within a fixed outer radius; however, in the above torque equation, the number of electrodes is factored into the overall expression by their method of integration. A close estimate of the number can be found by applying the equation below.

$$N_e = \frac{2\pi Ri}{p/2} \tag{79}$$

The derivation presented by the AT&T group is based on several assumptions that do not apply to the actuator design. Among the points of particular interest are:

1. The capacitance equation is only valid for areas with perimeter dimensions that are much greater than the plate separation distance. The proposed motor electrodes are six microns wide with a vertical separation of one micron.

2. The capacitor equation and thus the subsequent energy equation assumes no variation in the electric field over the plate area. For the given ratio of width to gap size, the electric field is more like that of dipole than the presumed linear form.

3. Using the method of partials to find the force equation is valid only for plates that fully overlap and have very small displacements of one plate compared to another. Their model is based on a one third overlap of the plates as the only contributing factor to the capacitance while the proposed motion spans the range of two electrode widths.

4. The torque equation is written under the condition that the drive force is always perpendicular to the radial arm. This assumption of only near interaction between the electrodes is consequentially based on the original calculation method for the force. Since all regions of the electrodes interact, the force varies in direction along full length.

Neither the article nor the patent mention optimization of the electrode pattern. In fact, the equations and methods of the AT&T design team do not allow the prediction of an optimum electrode pattern. As part of a design selection criterion they mention the outer region of the electrodes contributes more to the torque than the inner region. An example is given in which the ratio of outer to inner radius is set at 0.7 to give a torque prediction that is two thirds of the maximum. However, the equation and the comparison are

obviously wrong because the formula predicts the maximum torque occurs when the inner radius is zero.

The presumptions in the AT&T presentation of a silicon based micromotor are sufficient for an initial investigation into the functional characteristics of an electrostatic motor constructed using modern fabrication methods. However, as much as the new features of the motor overcome the classic limitations on fabrication, the need for a more accurate output prediction method is clear and without the selection of the optimum electrode pattern, the motor still lacks a superior performance when compared to existing electromagnetic motors.

The Rotation Rate Equation

For all variable capacitance electrostatic motors, the rotation rate is directly dependent on the number of electrode groups and the voltage driver's switching frequency. Once the actuation voltage is applied to induce motion, the drive voltage controller changes the electrode polarity when they realign. This switching time interval is related to the drive frequency by Equation 80.

$$f_s = \frac{1}{T_s} \tag{80}$$

The angular rotation rate can be derived from the definition given as:

$$\omega = \frac{\Delta\theta}{\Delta T} \tag{81}$$

For the time interval Ts, the amount of rotation is simply the angle between adjacent electrodes. Thus, the angular speed for the three phase case is given as:

$$\omega = \frac{2\pi/3N_g}{T_s} \tag{82}$$

Substitution of the drive frequency changes the Equation 82 to:

$$\omega = \frac{2\pi f_s}{3N_g} \tag{83}$$

Translation of the angle to one full rotation and the time interval into units of minutes gives the rotational speed (S) in rpms as:

$$S = \frac{20f_s}{N_g} \tag{84}$$

Thus, the rotation rate depends on the controller's drive frequency and the number of electrode groups in the motor. As the electrode fabrication width is reduced to produce a motor with a greater output, the drive frequency must be adjusted accordingly to yield the same rotation rate.

CHAPTER 4

THE OPTIMIZATION AND DESIGN PROCESSES

The versatility of the electrostatic actuator design allows the device to be shaped to fit within the space of the chosen application. Thus, the first step in the design procedure is the selection of the outer dimensions of the actuator housing. The second step is the selection of the fabrication method for production of the electrode pattern. The entire design parameterization of the motor and the optimization of the electrode pattern proceed from this initial information. Calculation of the torque for the rotary optimization process must be very accurate. For this reason the numerical method of the boundary elements is applied as the method of choice whenever the procedures call for a numerical result.

The Optimization Criteria for a Linear Electrostatic Actuator

To better understand the optimization process for a rotary electrostatic actuator, explanation of the design process for a linear actuator should be offered for comparison of the techniques. Since the linear actuator forms a rectangular box, the outer dimensions can be stated as length, width and height. The motion would typically be along the actuator length. The height determines the number of layers in the propulsion stack and the width determines the electrode length.

According to the force equation for the interaction between a pair of stator and slider electrodes the optimization of a linear electrostatic actuator is simple.

The force is maximized by:

1) maximizing the length of the electrodes.

2) minimizing the electrode width and spacing, and

3) minimizing the gap between the stator and slider.

Since the fabrication limits due to the flatness of the stator and slider material restrict the minimum size of the gap. the size of the electrodes and spacing is also restricted.

Egawa et al[13] suggest the electrodes and spacing be wider than the gap distance by a factor of at least 1.5. This ratio is a result of their studies into optimizing the performance of a linear actuator by experimentation. Thus. the optimization of a linear electrostatic electrode pattern is as follows:

1) the electrode length runs the full distance of the actuator's width.

2) the stator to slider gap is made as small as possible.

3) and the electrode width is set at 1.5 times the gap distance or greater.

The smaller the electrode width and spacing size. the greater the switching speed necessary to maintain the same linear speed of the slider. Since electronic circuits can run in the kilo. mega and even gigahertz range. it can safely be assumed that the drive speed can be made comparable by adjusting the circuit.

Thus. the limiting criteria set forth above are all that is needed for achieving the maximum possible force from a linear actuator that is designed to fit within a fixed space. The presumption that the fabrication limit is greater than the gap distance is practical for the state of the art in photo lithographic etch processing.

The Optimization Process for a Rotary Actuator

The process for optimization of the output from an electrostatic motor is the recognition that for a fixed electrode fabrication width, numerous radial patterns can fit within a given outer radius. The question then is which pattern should be used to produce the "best" motor. For any rotational motor, the output torque and energy efficiency are the two major parameters that determine design quality. Thus, the best motor is one that produces the highest possible torque while maintaining the greatest possible energy efficiency. This optimum electrode pattern is based on finding two parameters: the number of electrode groups and the electrode shape angle.

Examination of every possible electrode pattern is not necessary. To reduce the number of calculations, the torque is estimated for patterns determined by selecting the number of electrode groups as a percentage of Ngmax and then as a percentage of the remaining portion. Finally, Ng is stepped one value at a time until the peak torque is found.

The input parameters from the design procedure are: Np, Ro, s, z, εz, and V.

1. Determine the maximum number of electrode groups.

$$N_{g_{max}} = \frac{\pi}{2N_p ArcSin(s/2R_o)}$$

(Ngmax is truncated to the nearest integer.)

2. Set the number of groups to forty percent of the maximum number.

$$N_g = 0.4 * N_{g_{max}}$$

3. Calculate the number of electrodes.

$$N_e = N_p N_g$$

4. Calculate the electrode angle.

$$\theta_e = \frac{2\pi}{2N_e} = \frac{\pi}{N_e}$$

5. Calculate the inner electrode radius.

$$R_i = \frac{s}{2Sin(\theta_e/2)}$$

6. Calculate the torque using the design parameters. (Ng, Ro, Ri, θe, z, εz, V)
7. Record the value of the predicted torque.
8. Compare the current torque value with the previous value. If it is larger, increase the number of groups by ten percent of Ngmax and return to Step 3.
9. Now that the torque magnitude has deceased, reduce the value of Ng by 10% of the last step difference and run the process through Steps 3 to 7 until the torque magnitude decreases.
10. Increase the value of Ng by one and process through Steps 3 to 7 until the torque magnitude decreases again.
11. The value of Ng just before the decrease is the number of electrode groups that delivers the highest possible torque for the radial electrode shape.

Once the optimum number of electrode groups is found using the radial electrode shape. the effect of the shape angle variation can be restricted to only the neighboring values of Ng. Using the accumulated data on the electrode dimensions. continue the calculation of torque with the shape angle as one of the variable parameters. For each value of Ng, a single value of the shape angle will give the highest torque output. Compare the torque values for neighboring values of Ng until the peak is found. Now return to the design procedure.

The Design Procedure for a Linear Electrostatic Actuator

1. Determine the outer dimensions for the actuator housing. (Lh. Wh. Hh)
2. Based on the housing fabrication process. set the shell thickness. (Th)

$$L_p = L_h - 2T_h$$

$$W_p = W_h - 2T_h$$

$$H_p = H_h - 2T_h$$

3. Calculate the maximum length and width of the stator and the maximum thickness of the motor stack. (Lp. Wp. Hp)Determine the maximum length of the electrode. (Ws > Le)

$$L_e = k_e W_p$$

An electrode length factor (ke) can be set at any practical value. (i.e. 0.95)

4. Select the stator and rotor base board. (Tb, Tc)

5. Select the dielectric coating process for the electrodes. (Td)

6. Calculate the total thickness of the stators and rotors. (T)

$$T = T_b + 2T_d$$

7. Determine the gap distance between the rotor and the stator. (g)

8. Calculate the number of stators and sliders in the stack. (Ns, Nsl)

$$N_s = \frac{H_p - (T + 2g)}{2(T + g)}$$

$$N_{sl} = N_s + 1$$

(Truncate Ns to the nearest integer.)

9. Calculate the electrode width. (We)

10. Produce the electrode pattern for the etch process.

11. Form the electrode pattern on the based board.

$$W_e \geq 1.5 * g$$

12. Apply dielectric coating.

13. Cut the stator and slider patterns around the electrode patterns.

14. Assemble the actuator.

The Design Procedure for a Rotary Actuator

The design steps include only the specification of the parameters needed to construct an electrostatic motor using the optimized electrode pattern. All other ancillary steps and processes are common and considered obvious to an experienced engineer.

1. Set the outer dimensions of the motor housing. (Lh, Dh)
2. Based on the housing fabrication process chosen, set the shell thickness. (Th)
3. Calculate the maximum diameter of the motor's stator and the maximum thickness of the motor stack. (Dso, Lp)

$$D_{so} = D_h - 2 * T_h$$

$$L_p = L_h - 2 * T_h$$

4. Determine the outer radius of the electrode pattern. (Dso > 2Ro)

$$R_o = k_{eo}(D_{ro}/2)$$

An outer electrode radius factor (keo) can be set at any practical value. (i.e. 0.95)

5. Based on the etch fabrication process chosen, set the minimum line width for the electrodes and gaps. (s)
6. Select the stator and rotor base board. (Tb, Tc)
7. Select the dielectric coating process for the electrodes. (Td)
8. Calculate the total thickness of the stators and rotors. (T)

$$T = T_b + 2 * T_d$$

9. Determine the gap distance between the rotor and the stator. (g)

10. Calculate the number of stators and rotors in the

$$N_s = \frac{L_p - T - 2g}{2(T+g)}$$

$$N_r = N_s + 1$$

(Truncate Ns to the nearest integer.)

11. Calculate the vertical distance between stator and rotor electrodes.

$$z = g + 2(T_d - T_c)$$

12. Apply the optimization process with the parameters Np, Ro, s, z, and εz to determine the number of electrode groups (Ng) and the electrode shape angle (α).

13. Calculate the electrode angle and inner radius.

$$\theta = \frac{2\pi}{6N_g}$$

$$R_i = \frac{s}{2Sin(\theta/2)}$$

14. Determine the inner diameter of the stator. (2Ri > Dsi)

$$D_{s_i} = k_{s_i}(2R_i)$$

An inner stator diameter factor (ksi) can be set to any practical value. (i.e. 0.95)

15. Determine the rotor inner diameter. (Dsi >Dri)

$$D_{r_i} = k_{r_i} D_{s_i}$$

An inner rotor diameter factor (kri) can also be set to any practical value. (i.e. 0.95)

16. Produce the electrode pattern for the etch process.

17. Form the electrode pattern on the base board and apply the dielectric coating.

18. Cut the stator and rotor patterns around the electrode patterns.

19. Construct the shaft unit to match the rotor inner diameter and stack length.

20. Assemble the parts.

CHAPTER 5

A NUMERICAL OPTIMIZATION EXAMPLE

The design process of an electrostatic motor that can fit in the housing of an electromagnetic motor that is currently on the market is given here. The Micro Mo Electronics, Incorporated[29] company manufactures small and miniature electromagnetic motors. Their Series 1212 micromotor is selected for comparison. It has the parametric characteristics stated as follows:

Housing Length: Lh = 12 mm

Housing Diameter: Dh = 12 mm

Stall Torque: τ = 0.034 in-oz

The fabrication process for printed circuit boards as employed by Dynamics Research Corporation[24] allows the reasonable presumption of fabrication parameters as follows:

Fabrication Width: s = 50 μm

Base Board Thickness: Tb = 100 mm

Conductor Thickness: Tc = 12 μm

Dielectric Coating Thickness: Td = 20 μm

Vertical Gap Separation: g = 14 μm

The work by Niino et al[14] provides working values for the electric permittivity of the electrode coating and the lubricant.

Dielectric Coating Permittivity: $\varepsilon d = 3.5 * \varepsilon o$

Lubricant Permittivity: $\varepsilon g = 1.9 * \varepsilon o$

Under the presumption of common circuit capabilities, the controller parameters are chosen to present an average electric potential of half the peak voltage of a normal house outlet with a three phase switching pattern.

Voltage: V= 60 Volts

Number of Phases: Np = 3

The calculations for the steps outlined in the design procedure for an optimized rotary actuator are repeated here with the numerical data included. To reduce the complexity of this example, the electrode shape angle parameter is not used in the optimization process.

The Design Procedure for a Rotary Actuator

1. Set the outer dimensions of the motor housing.

Lh = 12 mm

Dh = 12 mm

2. Based on the housing fabrication process chosen, set the shell thickness.

Th = 0.5 mm

3. Calculate the maximum diameter of the motor's stator and the maximum thickness of the motor stack.

$$Dso = 12 - 2*0.5 = 11 \text{ mm}$$

$$Lp = 12 - 2*0.5 = 11 \text{ mm}$$

4. Determine the outer radius of the electrode pattern.

$$Ro = 0.9*5.5 = 4.95 \text{ mm} \sim 5 \text{ mm}$$

5. Based on the etch fabrication process chosen, set the minimum line width for the electrodes and gaps.

$$s = 50 \ \mu m$$

6. Select the stator and rotor base board.

$$Tb = 100 \text{ mm}$$

$$Tc = 12 \ \mu m$$

7. Select the dielectric coating process for the electrodes.

$$Td = 20 \ \mu m$$

8. Calculate the total thickness of the stators and rotors.

$$T = 100 \ \mu m + 2*20 \ \mu m = 0.14 \text{ mm}$$

9. Determine the gap distance between the rotor and the stator.

$$g = 14 \ \mu m$$

10. Calculate the number of stators and rotors in the stack.

$$Ns = (11 - 0.14 - 2*0.014) / (2*(0.14 + 0.014)) = 35$$

$$Nr = 35 + 1 = 36$$

11. Calculate the vertical distance between stator and rotor electrodes.

$$z = 14 + 2 * (20\text{-}12) = 30\ \mu m$$

12. Apply the optimization process with the design parameters Np, Ro, s, z, εz and V to determine the number of electrode groups.

$$Ng = 56$$

$$\tau = 1.514\ \text{mN-mm} = 2.144\text{E-}4\ \text{inch-oz}$$

(The process is described in detail below.)

13. Calculate the electrode angle and inner radius.

$$\theta = (2\ \pi) / (6*56) = 0.0187\ \text{rad} = 1.071^{\circ}$$

$$Ri = 0.05 / (2*\text{Sin}(\ 0.0187/\ 2)) = 2.674\ \text{mm}$$

14. Determine the inner diameter of the stator.

$$Dsi = 0.9*(\ 2 * 2.674) \sim 4.8\ \text{mm}$$

15. Determine the rotor inner diameter.

$$Dri = 0.95 * 4.8 = 4.56\ \text{mm}$$

16. Produce the electrode pattern for the etch process.

17. Form the electrode pattern on the base board and apply the dielectric coating.

18. Cut the stator and rotor patterns around the electrode patterns.

19. Construct the shaft unit to match the rotor inner diameter and stack length.

20. Assemble the parts.

This procedure ends with the two construction phases of etching electrode pattern chosen by the optimization processing on the base board material of the stators and rotors and then assembling motor as shown in Chapter 2.

The Optimization Process for a Rotary Actuator

The input begins by passing the fixed parameters determined in the design procedure.

$Np = 3$
$Ro = 5$ mm
$s = 50$ μm
$z = 30$ μm
$\varepsilon z = \varepsilon o = 8.85E\text{-}12$ F/m

1. Determine the maximum number of electrode groups.

$$Ngmax = \pi / (2*3*\text{ArcSin}(.05 / (2*5))) \sim 104$$

2. Set the number of groups to forty percent of the maximum number.

$$Ng = 0.4 * 104 = 40$$

3. Calculate the number of electrodes.

$$Ne = 3*40 = 120$$

4. Calculate the electrode angle.

$$\theta e = p/120 = 0.02618 \text{ rad}$$

5. Calculate the inner electrode radius.

$$Ri = 0.05 / (2 \text{ Sin}(0.02618/2)) = 1.90991 \text{ mm}$$

6. Calculate the torque using the design parameters. (Ng, Ro, Ri, θe, z, εz, V)

(The values are applied in the COULOMB program to produce the electrode pattern for calculation of the total torque on the rotor.)

7. Record the value of the predicted torque.

$$\tau = 1.382 \text{ mN-mm}$$

8. Compare the current torque value with the previous value. If it is larger, increase the number of groups by ten percent of Ngmax and return to Step 3. In the first pass, the previous value is coded as zero, so the first torque value is higher.

Steps 3 through 8 are repeated with the input data given in Table 5 and the predicted torque plotted in Figure 29.

Table 5 Input Parameters for Steps 3 to 8

Ng	40	50	60	70	80
θe	1.500	1.200	1.000	0.857	0.750
Ri	1.910	2.387	2.865	3.342	3.820

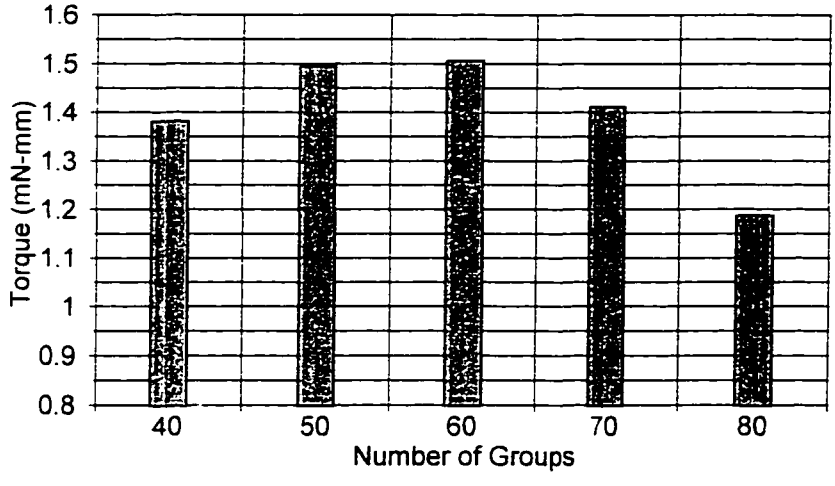

Figure 29 Coarse Torque Data

The chart clearly shows that a peak value will occur when the number of electrode groups is between 50 and 60. The search process is refined in the next step.

9. Now that the torque magnitude has deceased, reduce the value of Ng by 10% of the last step difference and run the process through Steps 3 to 7 until the torque magnitude decreases.

10. Increase the value of Ng by one and process through Steps 3 to 7 until the torque magnitude decreases again.

11. The value of Ng just before the decrease is the number of electrode groups that delivers the highest possible torque for the radial electrode shape.

To demonstrate the method further, the value of Ng will be varied about 60 instead of following steps 10 and 11 precisely. This will show a clear trend in the torque curve. As above, the input data is given in the table and the output torque is presented in a chart.

Table 6 Input Parameters for Steps 9 to 11

Ng	54	55	56	57	58	59	60	61	62	63
θe	1.111	1.091	1.071	1.053	1.034	1.017	1.000	0.984	0.968	0.952
Ri	2.578	2.626	2.674	2.722	2.769	2.817	2.865	2.913	2.960	3.008

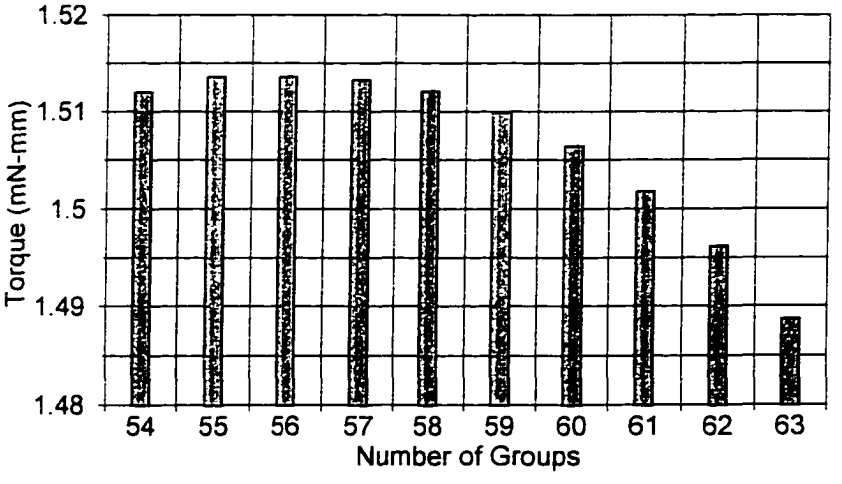

Figure 30 Refined Torque Data

The peak torque occurs when the number of groups is 56. For this case, the difference between the torque for Ng equals 55 and 56 is very small and thus can not be clearly read from the chart. The value of 56 was chosen from the numerical data. The trend in torque values is unmistakably towards the maximum at particular value of the number of electrode groups.

Using the parametric values determined from the optimization process and the electrode scheme presented earlier, the electrode pattern can be produced as shown in Figure 31. Since every third electrode must be connected, a conducting ring is etched around the inner perimeter for the first electrode set and a conducting ring is etched around the outer perimeter for the third electrode set, while the middle electrodes are connected by a ring embedded in the base board material.

Figure 31 Optimum Electrode Pattern

The Output Comparison

Since the torque calculations with the COULOMB program used the electric permittivity of free space. the torque magnitude needs to be adjusted to account for the layers of dielectric material between the stator and rotor electrodes. The equivalent dielectric permittivity is simply the layered dielectric constant times the free space permittivity. Thus the equivalent dielectric constant is given by changing the terms of Equation 7 to dielectric constants.

$$k_z = \frac{z}{\frac{g}{k_g} + \frac{2(t_d - t_c)}{k_d}} \qquad \textbf{(85)}$$

Calculation of the layered constant is then written as:

$$kz = 30 / (14/1.9 + 2(20-12)/3.5) = 2.51$$

The peak torque output which was predicted in the design procedure is adjusted by direct multiplication of the layered constant to give the true value for the functioning motor. This value is then multiplied by the number of electrode pattern interactions which is twice the number of rotors. to given the total motor output.

$$(kz\ \tau)\ (2\ Nr) = 2.51 * 2.144E\text{-}4 * 2 * 36 = 0.03875 \text{ in-oz}$$

This value is greater than the stall torque for the comparable electromagnetic motor.

CHAPTER 6

DATA ANALYSIS AND METHODOLOGY

The specific design process presented in Chapter 5 serves as a simplified example to demonstrate the optimization process. The extent of the procedure necessary to determine the optimum design depends on the degree of the model's accuracy and the level of parametric variations the investigator wishes to include. A complete optimization would involve evaluating the effect of each parameter and including all electrically active materials in the numerical torque calculations. The details of the numerical analysis and the discovered advances in the design methodology are presented below through the descriptions of several models chosen for study.

The fundamental parametric values for the series of models investigated to prove the optimization criteria are listed in Table 7. The basic optimization process for the third model in the table is described in Chapter 5. The resultant information given in the previous description is repeated in this chapter for continuity.

Table 7 Model Parameters

Outer Radius (mm)	Fabrication Width (μm)	Vertical Gap (μm)
5	100	50
5	75	40
5	50	30
5	25	20
2.5	25	15
2.5	6	1

The last model in Table 7 is for comparison to the Gabriel et al predictions. Each model has its own set of graphs to illustrate the predicted effect of the chosen parameters. The models are described in order of convenience as given by the titles.

Model 5-50-30: Ro= 5 mm, s = 50 μm, z = 30 μm

The first step in determining the optimum parametric design is to plot the torque against the number of electrode groups to locate the maximum value. For most graphs, only one parameter is changed while all the others are held constant. Figure 32 shows the change in predicted torque output with a change in the number of electrode groups. The coarse spacing between the Number of Groups is to reduce the amount of calculations for a single parameter. Here, the predicted maximum lies between 60 and 70 electrode groups.

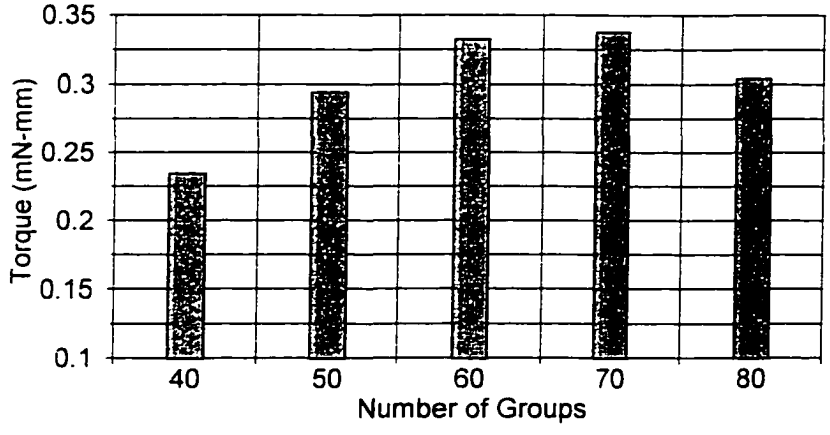

Figure 32 Coarse Torque Data

The torque prediction given in Figure 32 presumes the stator and rotor are in their initial positions. However, the torque changes as the rotor turns. An angular displacement

of twice the electrode width results in realignment of the electrodes. Thus, Figure 33 shows a sample plot of the torque variation with angular position (Ψ) for the case of 60 electrode groups.

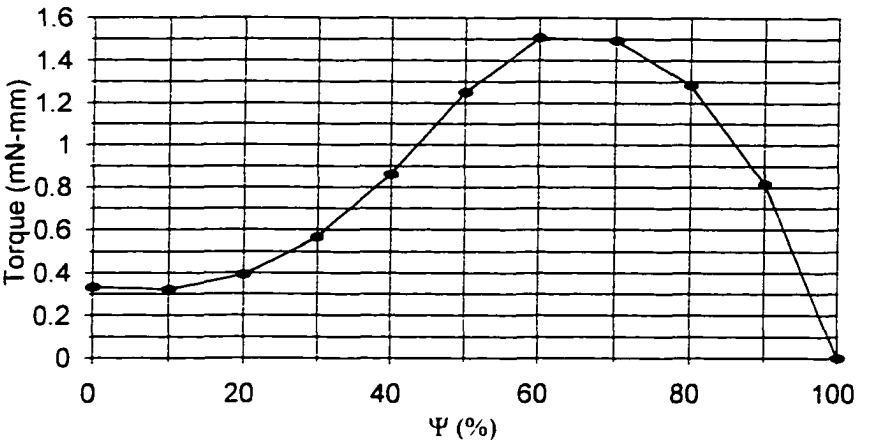

Figure 33 Torque versus Rotor Position

This shows that the peak torque occurs at approximately 60% of the realignment rotation distance. This maximum value is about five times greater than the initial magnitude. As a check of the methodology, the torque is plotted against the Number of Groups for the case of the rotor turned to the peak torque position.

Figure 34 shows that for the rotated case, the maximum torque occurs between 50 and 60 electrode groups. This is a significantly different location from the first prediction. Now a decision must be made between the two possible criteria for optimization.

Integration of the torque data over the angular displacement multiplied by the number of electrode groups gives the total work done by the rotor per revolution. Using the

work per revolution criteria, another condition for optimization can be introduced for the investigation. This data is shown in Figure 35.

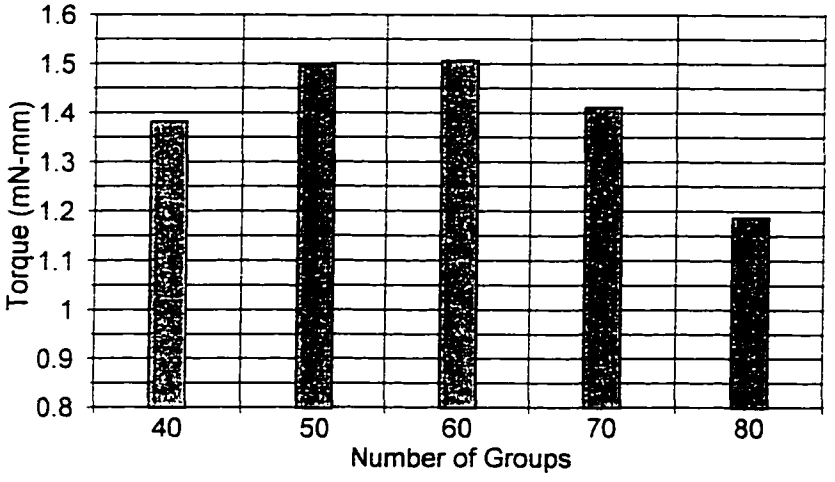

Figure 34 Torque Plot at 60% Rotation

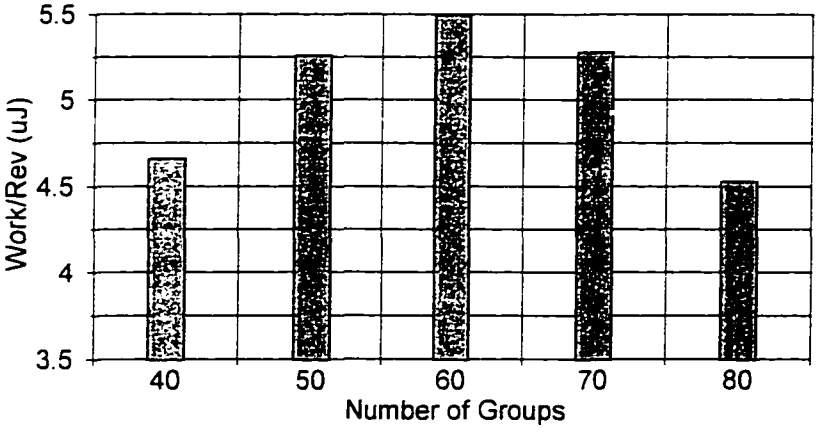

Figure 35 The Work per Revolution Data

This plot shows yet another possible choice of the number of groups that yields the maximum output for the motor. Here, the optimum number of groups is between 60 and

70 but is likely to be closer to 60 than the prediction using the initial value for the torque. To refine the predictions, the torque is calculated using a single step in the number of groups for each of the criteria given above in Figures 32, 34 and 35. These data are shown in Figures 36, 37 and 38, respectively.

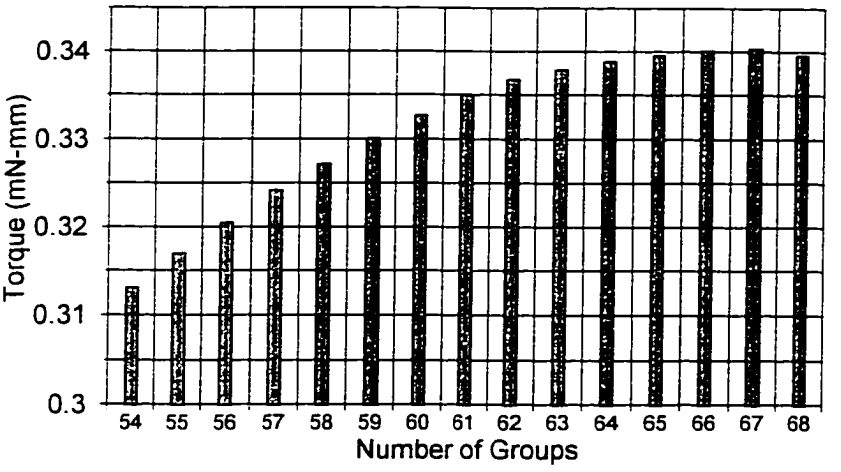

Figure 36 Refined Torque Data for Initial Rotor Position

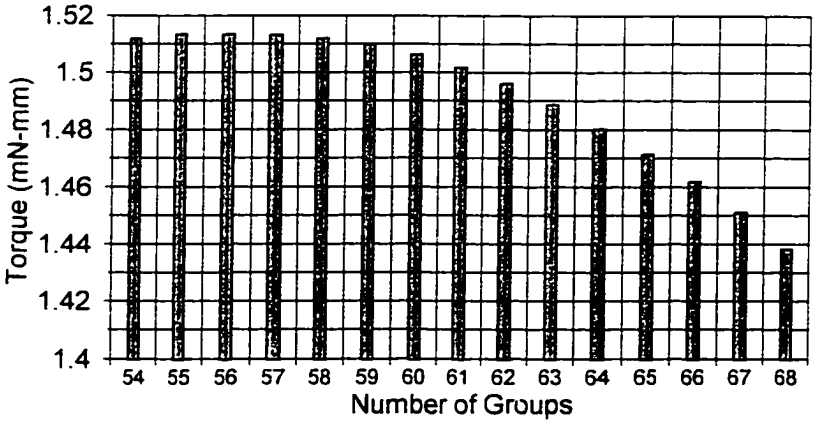

Figure 37 Refined Torque Data for 60% Rotation

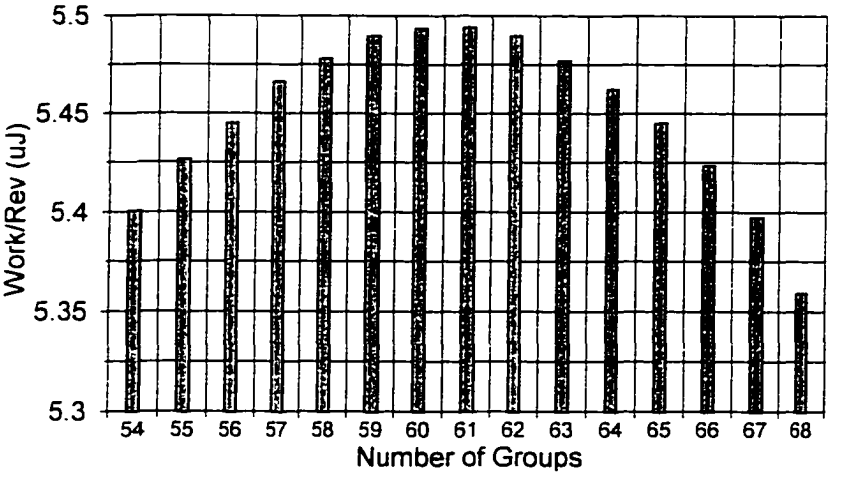

Figure 38 Refined Work per Revolution Data

For the three cases shown above, the maximum value of the output occurs when the number of electrode groups is at 67, 56 and 61, respectively. Now, one of the criteria must be chosen as the best for optimization of the motor. This decision can be assisted by plotting the three data curves together using normalized magnitudes as shown in Figure 39.

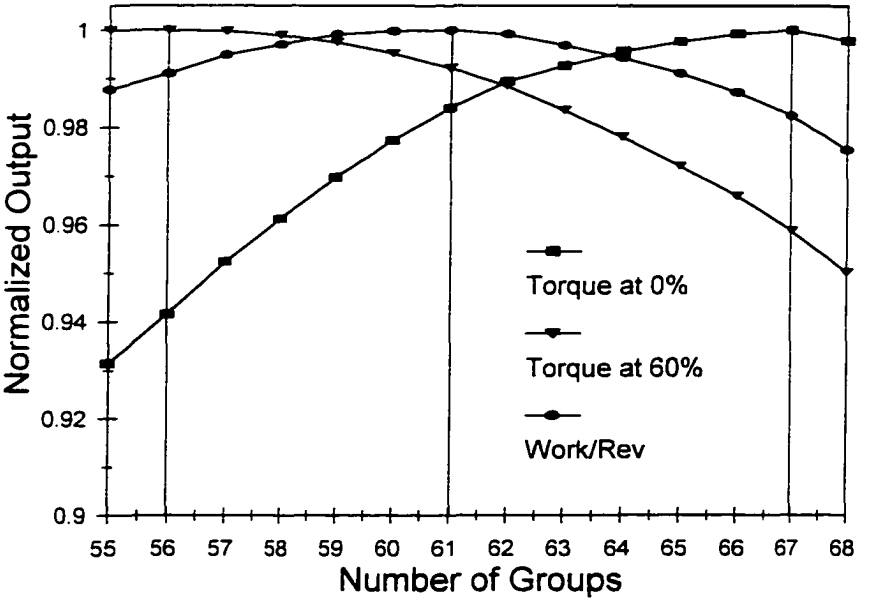

Figure 39 Normalized Output Data

From the combined graphs, the values of each variable can be selected for the number of electrode groups corresponding to the maximums. This information is compiled in Table 8.

Table 8 Normalized Peak Data Points

	Torque at Ψ= 0%	Torque at Ψ=60%	Work per Revolution
Torque at Ψ=0%	100%	95.8%	98.3%
Torque at Ψ=60%	94.2%	100%	98.4%
Work / Revolution	98.4%	99.2%	100%

The last column shows that selection of the work per revolution criterion gives the highest percentages for initial and peak torques. However, if the peak torque criteria is chosen, the work per revolution will have its highest values as a secondary parameter. The investigator must choose which conditions are best to provide the optimum motor output.

For the example in Chapter 5, the torque at 60% rotation was chosen as the optimum method because the comparison with a conventional motor was based on the maximum torque output. As an overall rule, the energy efficiency is more important for a long duration motor and thus the work per revolution criterion should be selected. This latter case is suggested by the author as the preferred method for choosing the optimum design. For simplicity, most of the remaining evaluations are based on maximizing the torque. Extrapolation to the energy efficiency method is obvious given the information above.

The other major parameters investigated include the electrode shape angle and the vertical gap distance. Both the these affect the output but only the shape angle shows the characteristic peak curve.

The Electrode Shape Angle Effects

For any chosen value of the number of electrode groups, the shape angle can be varied to show its effect on the peak output. Figure 33 shows the torque variation with rotor position. Similarly, Figure 40 shows the family of curves resulting from a change in the electrode shape angle (α) for the case 55 electrode groups. The angle is varied from zero to θ as described in Chapter 2 using Figure 20.

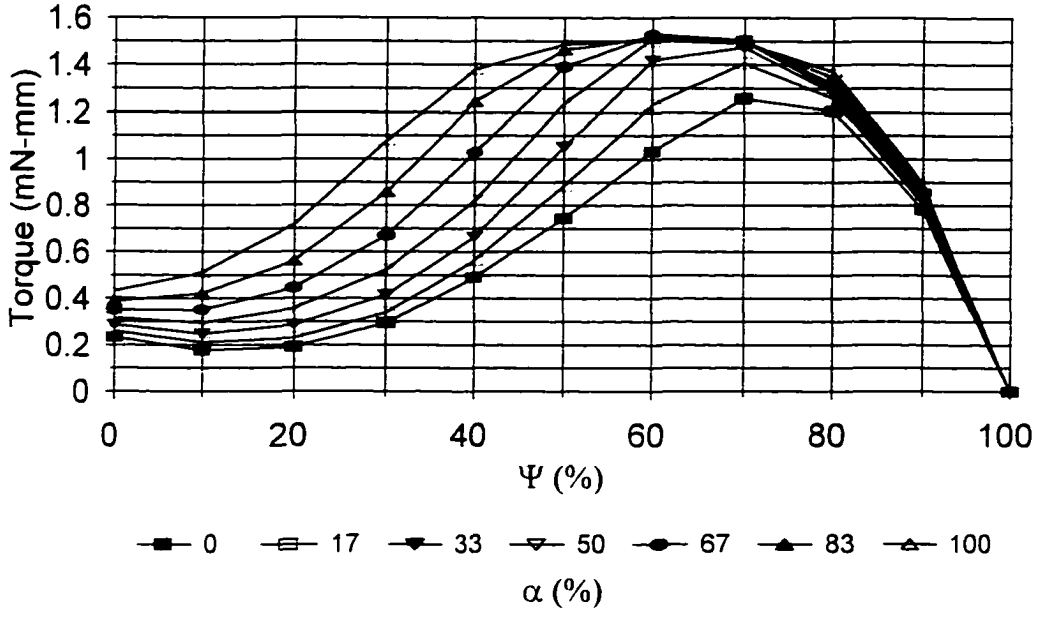

Figure 40 Shape Angle Curves

The peak torque for each of the curves varies both in magnitude and in rotational position. To help distinguish the major features of the graph, the forth and last curves are re-plotted in Figure 41. Here, it is clear that the peak torque occurs at 60% rotation when α is about two thirds of θ; but more significantly, the area under the curve is much greater when α equals θ.

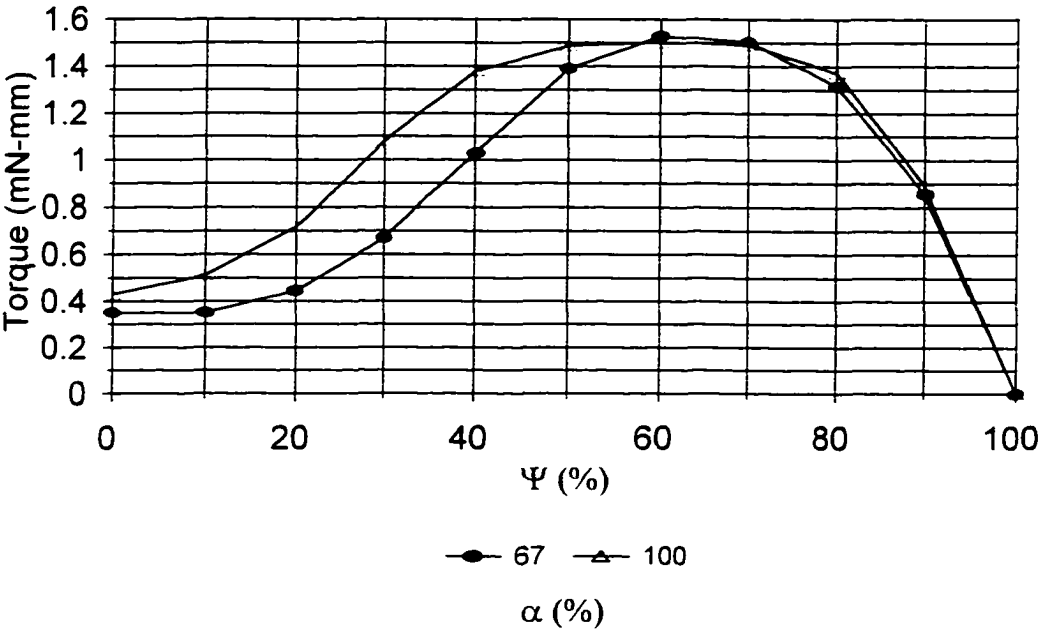

Figure 41 Peak Torque and Maximum Area Curves

To further demonstrate the effect of the shape angle on output, the curves in Figure 40 are integrated to yield the work per revolution as shown in Figure 42. This shows a monotonic trend in the shape angle effect on the work output. Clearly, the larger the shape angle the greater the energy efficiency of the motor.

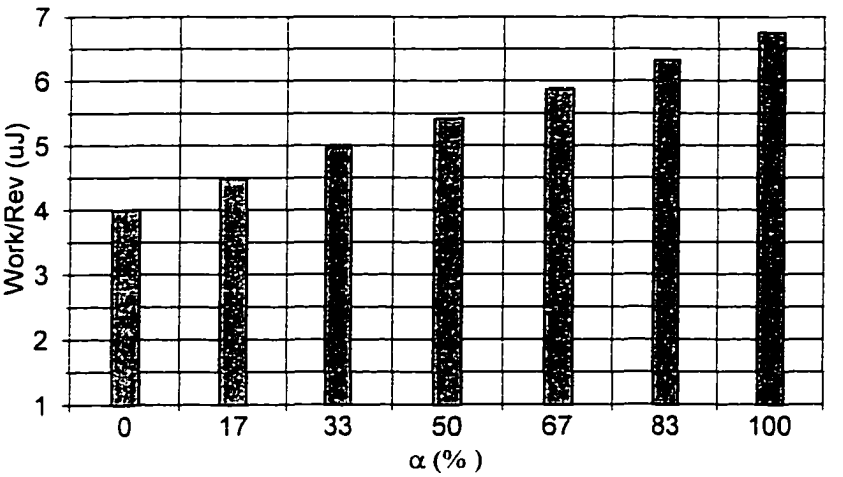

Figure 42 Shape Angle Effect on Work per Revolution

The Vertical Gap Effect

The separation distance between the stator and rotor can attain a minimum value depending the flatness of the interacting surfaces. The upper limit on the value of z is restricted by the fabrication accuracy which determines the electrode width. For the sake of this investigation, the gap is varied over a practical range to demonstrate its effect without regard for fabrication limits. Once the gap effect is understood, the application limits can be employed to determine the final design value.

Figure 43 shows a three dimensional plot of the torque variation over the rotation range with a change in the vertical gap distance. The shape of the curves is maintained for each of the gap values while the magnitude increases as the gap is narrowed for most of the rotational positions.

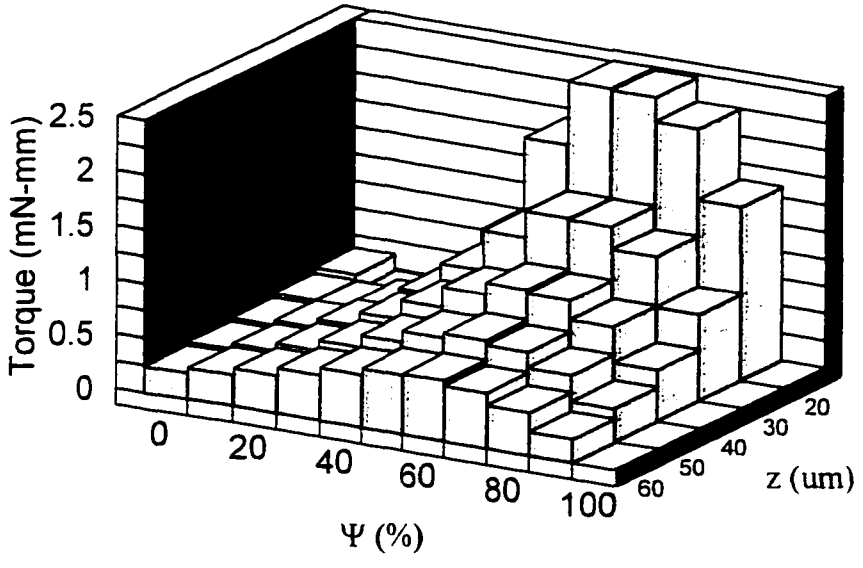

Figure 43 Effect of Gap Distance on Torque

Integration of the curves in Figure 43 over the rotation distance gives the work per revolution. Figure 44 shows the work data for each the selected gap values. This chart follows an exponential increase in work output as the gap deceases. Thus, Figures 43 and 44 lead to the conclusion that the smaller the gap between the stator and rotor the greater the peak torque and work output of the motor.

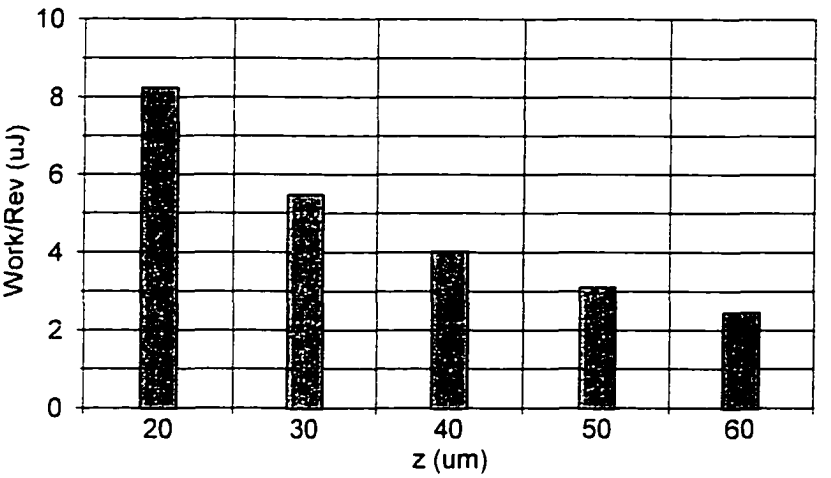

Figure 44 Work per Revolution Data

Since the gap should be made as narrow as possible, the criterion for selection of the value of z is strictly based on the fabrication method. With this knowledge, it is determined that the gap magnitude should be set in the initial design phase as a constant for the optimization process.

Note that the above gap distance plots are based on a fixed value of Ng equal to 63 with a radially shaped electrode. Other numerical investigations show this trend to be consistent regardless of the other parameter values.

Optimization with the Shape Angle Effect

Leaving the vertical gap distance at 30 microns, the optimum number of electrode groups is reevaluated with the shape angle set to its peak torque value of two thirds θ and the rotor turned to 60% of a rotation.

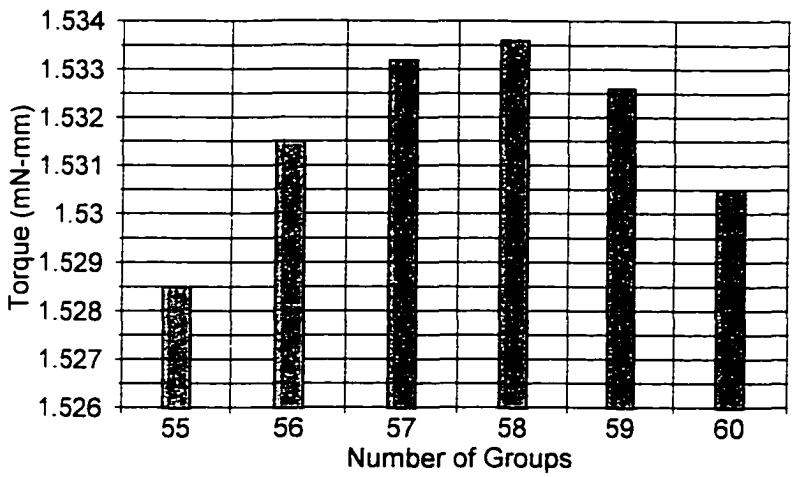

Figure 45 Shift in the Optimum Electrode Pattern

With a change in the shape angle, the maximum torque output is shifted from 56 to 58 electrode groups. The peak torque from Figure 37 is 1.5136 mN-mm while the peak from Figure 45 is 1.5336 mN-mm. This demonstrates the effect of the addition of the shape angle parameter as providing an increase of only 1.3 % in torque output. This small amount makes the shape angle a secondary parameter when compared to the total contribution of the number of electrode groups. None the less, true optimization of the electrode pattern should include the shape angle to help provide the greatest possible energy efficiency for an electrostatic motor.

Model 5-100-50: Ro= 5 mm, s = 100 μm, z = 50 μm

Following the pattern of investigation used for Model 5-50-30, another model can be examined with greater ease. Using the same outer radius, the previous model is modified presuming a less accurate fabrication process which can only provide an electrode spacing of 100 microns and a stator to rotor gap of 50 microns.

The first part of the process is to apply a coarse spacing to the number of electrode groups for each of the possible optimization conditions. For this model, only the two torque criteria are considered. Figures 46 and 47 show the output data for the initial rotor position and the 60% rotation position, respectively.

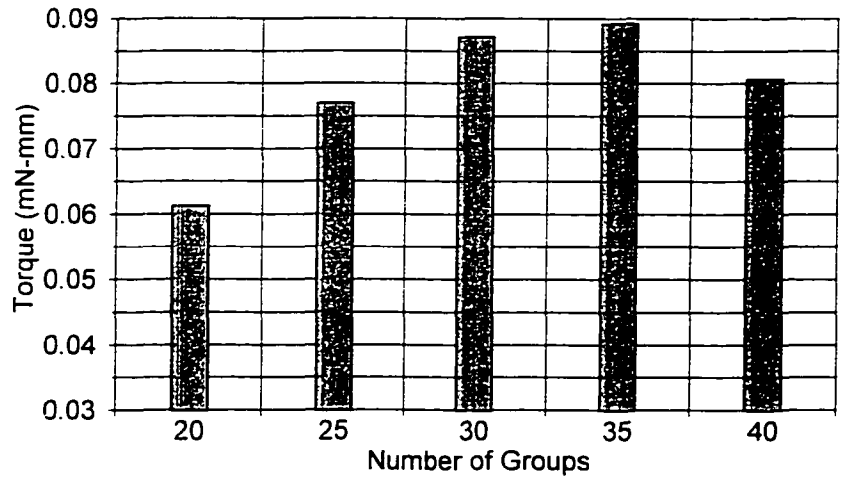

Figure 46 Torque Data for Initial Rotor Position

The charts show the optimum number of electrode groups to be between 30 and 35 for the first case and between 25 and 30 for second. Now the plots are refined to single spacing to locate the optimum.

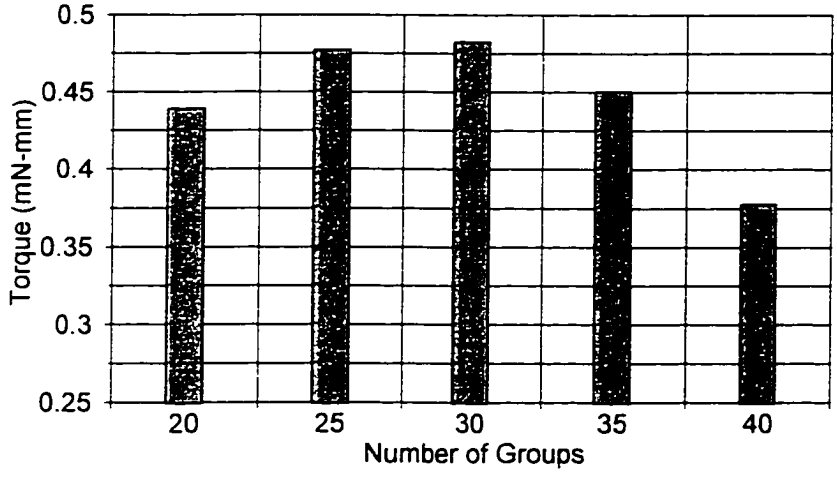

Figure 47 Torque Data for 60% Rotation

As an illustrative example. Figure 48 contains both the coarse and fine spacing for the number of electrode groups. From the extended data points in the graph. the trend towards a maximum is clearly defined. Here. the optimum number of electrode groups is predicted to be 33.

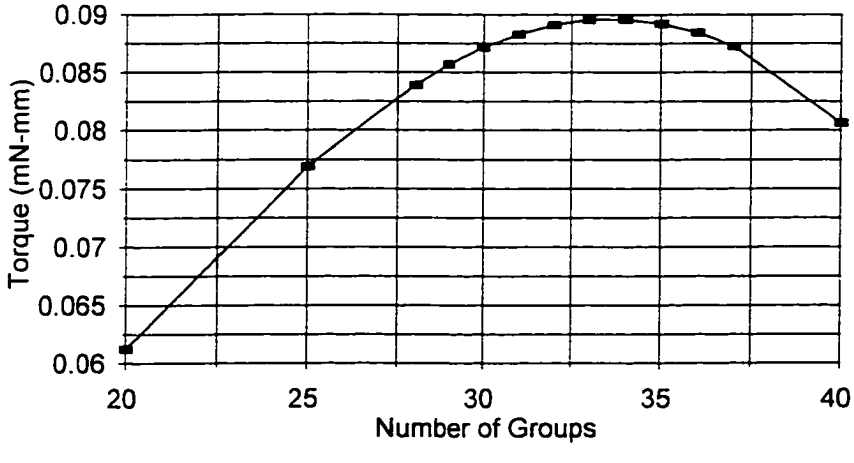

Figure 48 Extended Torque Data

As another example, the investigator can reasonably estimate the number of groups and thus reduce the number of simulations. Figure 49 shows the optimum number of electrode groups to be 28 for the 60% rotation case.

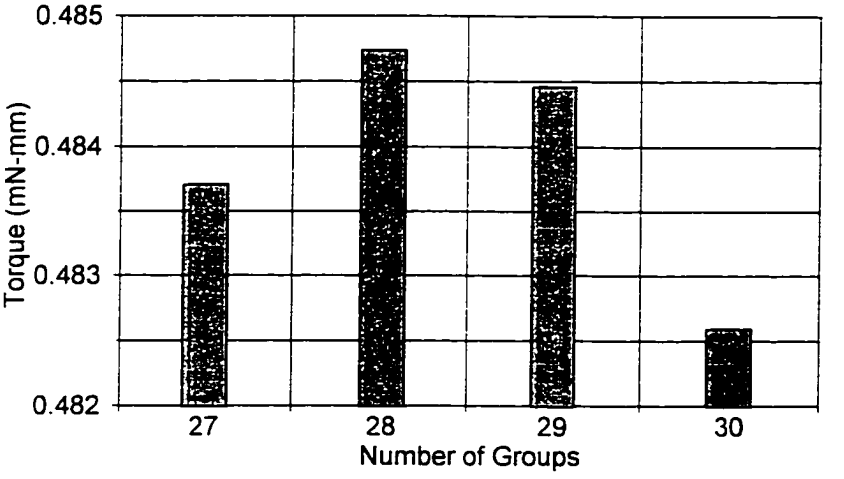

Figure 49 Torque Data for the 60% Rotation Case

Again, the question remains of which condition to choose as the best for predicting the optimum behavior of the motor. As with the first model, the torque at 60% rotation is considered the best case.

For the final step, the best electrode shape is presumed to be at α equal to two thirds of θ as was shown above. The model is then re-evaluated with the wider electrode. The torque data for this case is shown in Figure 50. The maximum output torque has increased and the optimum number of electrode groups has shifted to a higher number as before. This pattern indicates that future prediction of the model behavior may be simplified if this trend is found to be distinctive.

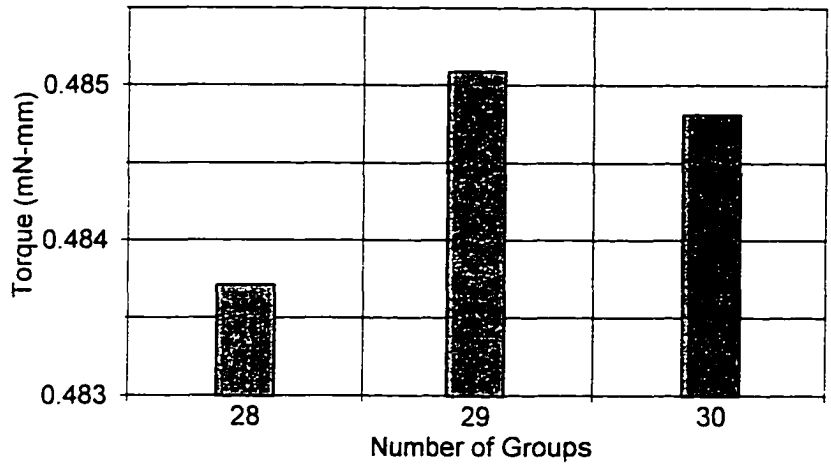

Figure 50 Torque Data for Wider Electrode

The Difference between Charge Patterns

All of the data simulations use the electrode charge pattern shown in Figure 28 as presented by the Egawa group. They also considered changing the polarity of the neutral stator electrode to negative. This would add a charge source that would either enhance or impede the torque on the rotor. Model 5-100-50. with its optimum number of electrode groups determined to be 28. is used to show the effect of changing the electrode charge pattern. Figure 51 shows the torque curves for the two cases.

The output for the new case is greater except at the initial position of the rotor. Otherwise. the additional charged electrode adds significantly to the torque output. Also. integration of the curves shows the work per revolution is 32% greater for the new charge pattern.

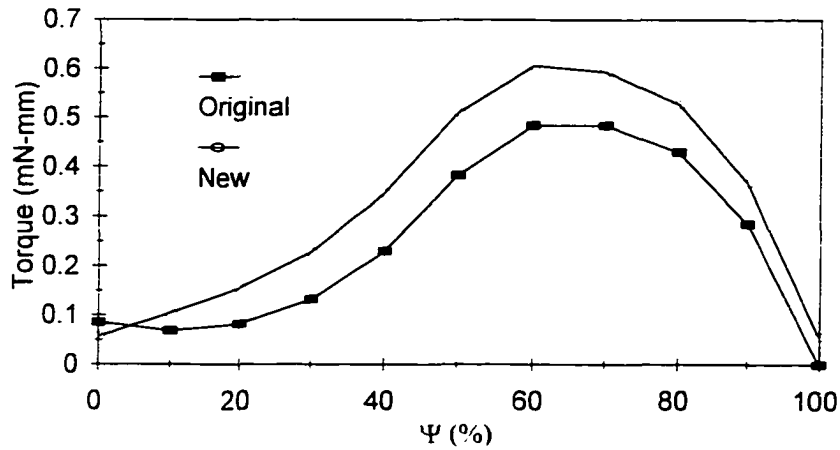

Figure 51 Comparison of Charge Pattern Effects

Model 5-75-40: Ro= 5 mm, s = 75 μm, z = 50 μm

With the method for prediction of the optimum number of electrodes groups demonstrated by two earlier models, the description for this model is shortened. Figures 52 and 53 contain the torque data for the 60% rotated case and the rotated case with the wider electrode. Figure 54 shows the optimum for the work per revolution condition.

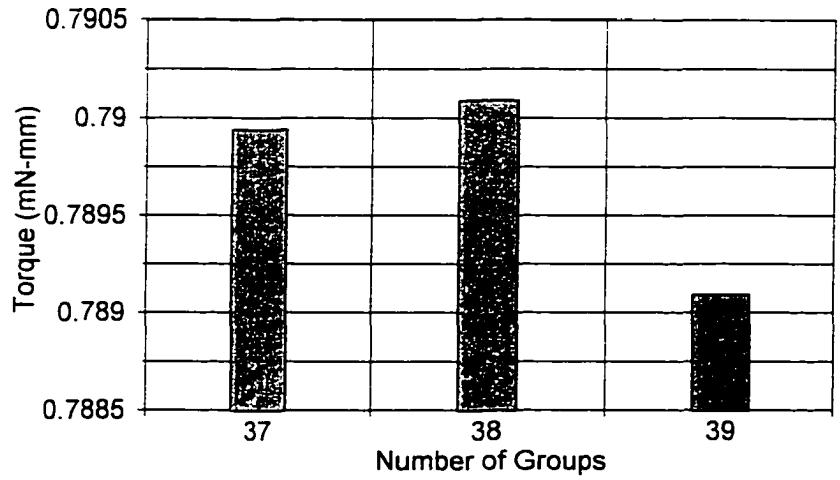

Figure 52 Torque Data for the 60% Rotation Case

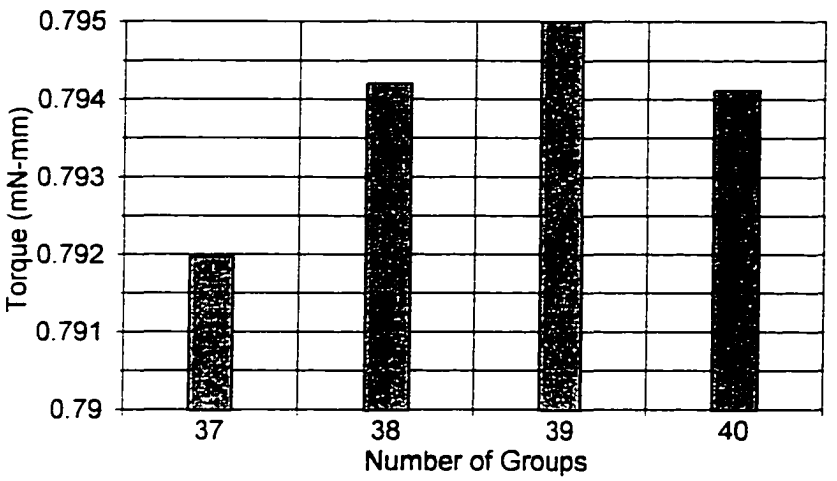

Figure 53 Torque Data for the Wider Electrode

As before, the wider electrode shifts the torque prediction to a higher value. For this case, the work per revolution is calculated using the wider electrode. The work condition now predicts the same optimum as the torque condition.

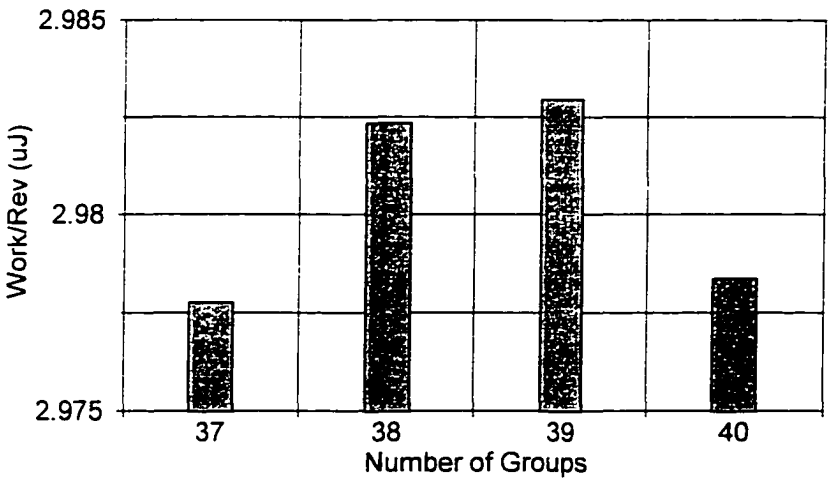

Figure 54 Work Data for the Wider Electrode

Model 5-25-20: Ro= 5 mm, s = 25 μm, z = 20 μm

Analysis of the optimum electrode pattern for this model follows that previous models by examining the torque for the rotated position and the work per revolution. The coarse and refined torque data is presented in Figures 55 and 56 respectively, while the corresponding work data are presented in Figures 57 and 58. The predictions are easily discerned as expected.

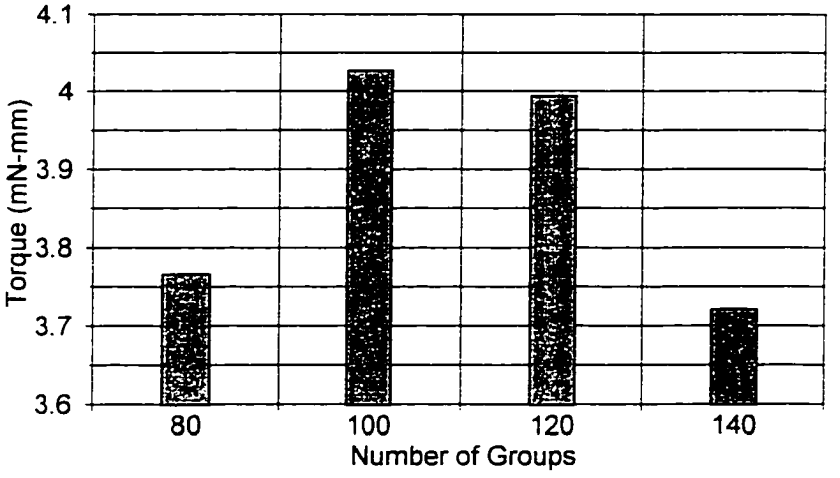

Figure 55 Coarse Torque Data

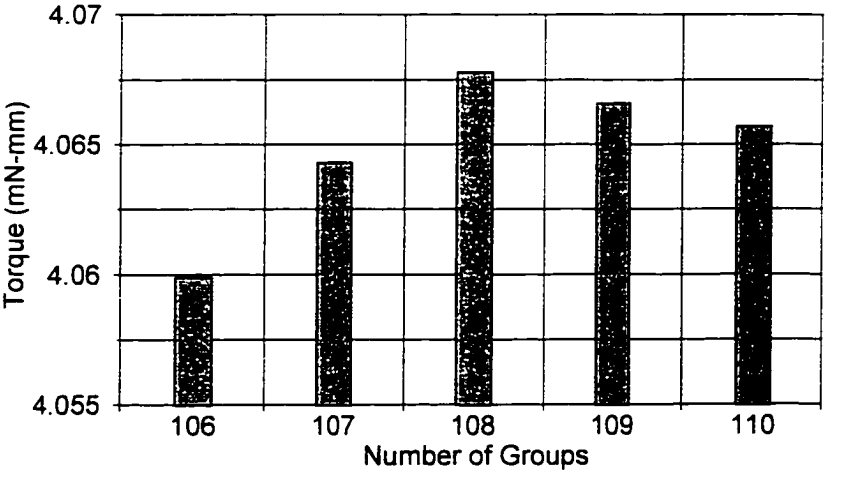

Figure 56 Refined Torque Data

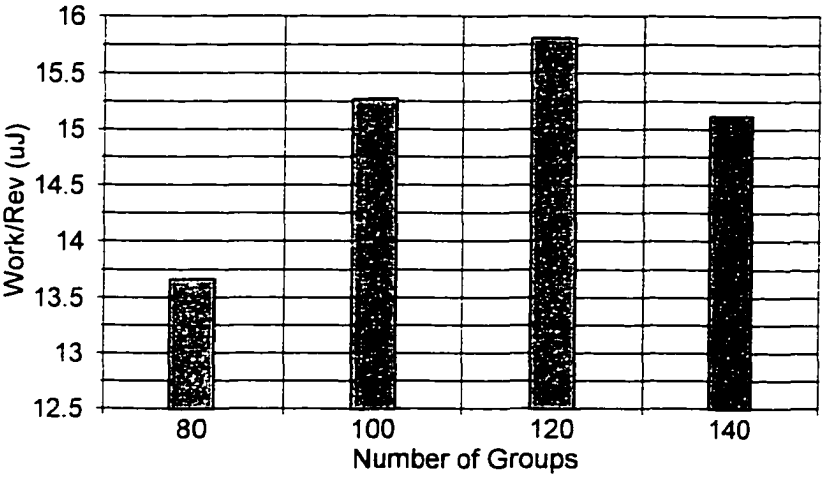

Figure 57 Coarse Work per Revolution Data

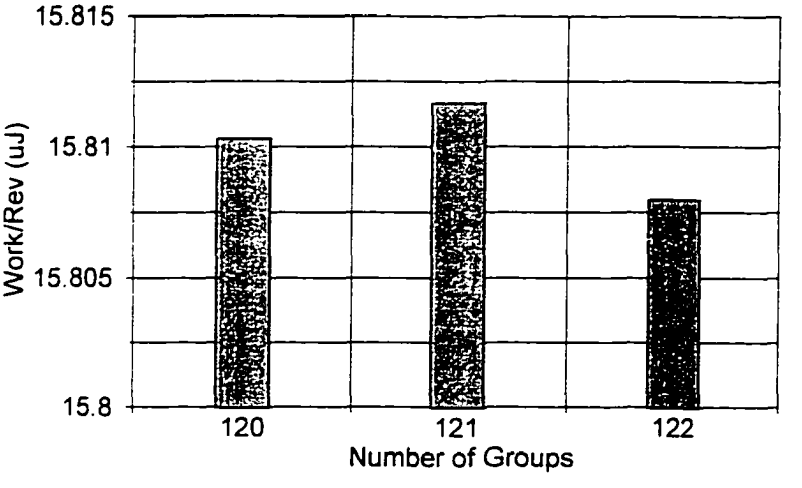

Figure 58 Refined Work per Revolution Data

The optimum predictions for the two cases are 108 and 121 electrode groups. These values are very nearly twice the values predicted for the first model which has an electrode fabrication width that is twice the size of this model. This suggests an approximate inverse relation between the two parameters.

Model 2.5-25-15: Ro= 2.5 mm, s = 25 μm, z = 15 μm

This model's basic parameters are all half the size of the first model. The coarse and refined torque data for the rotated case are given in Figures 59 and 60. The predicted optimum number of groups is the same as for the larger model. This suggests a direct correlation in scale.

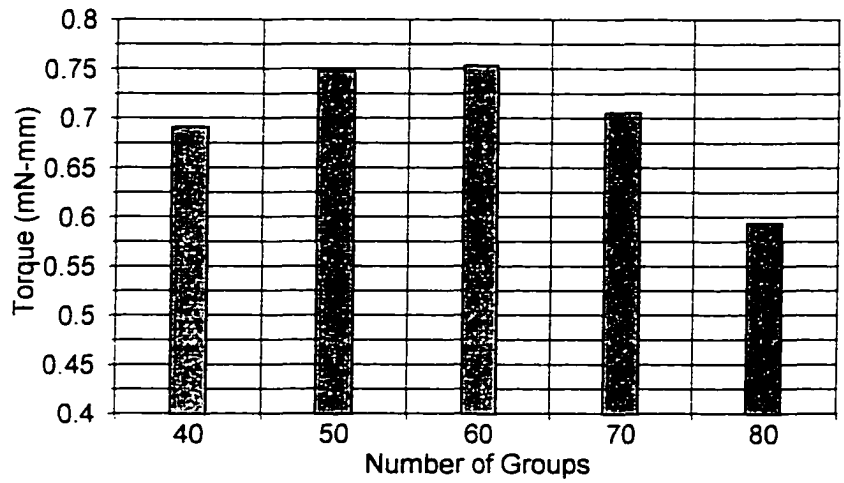

Figure 59 Coarse Torque Data

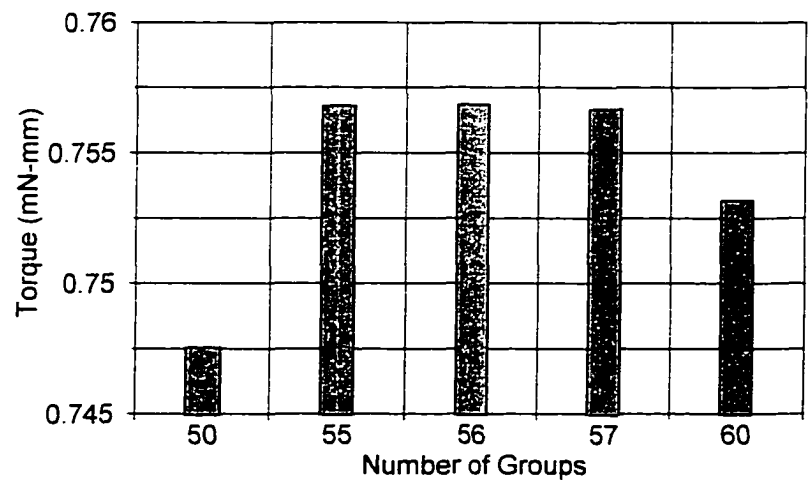

Figure 60 Refined Torque Data

Combination of 5 mm Radius Model Data

To show the effect of the electrode fabrication width on the output, the maximum torque for each of the optimized models with an outer radius of five millimeters is compiled into one graph. The data collected are from the simulations using the radial shaped electrodes with the rotor turned to the peak output position. The trend shown in Figure 61 appears to be either exponential or reciprocal in the fabrication width.

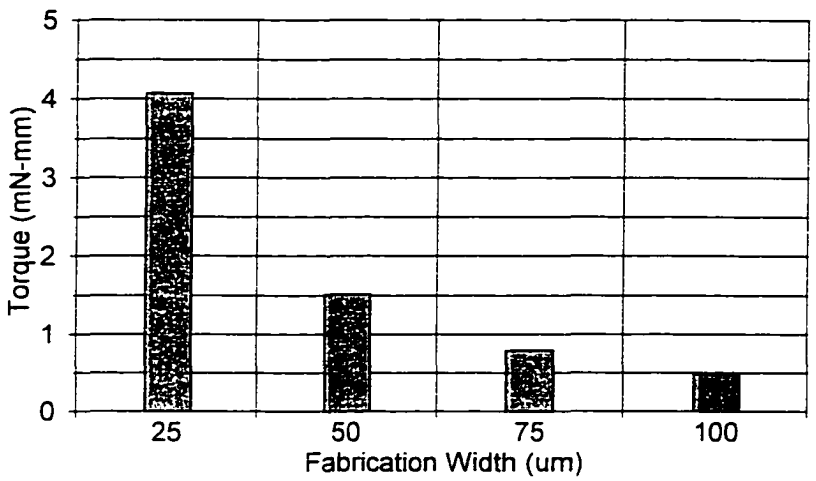

Figure 61 Combined Torque Data

The reduction in fabrication width from 100 microns to 25 microns results in increasing the torque by factor of eight. This change in the performance due to a change in the electrode width exemplifies the need of microfabrication methods to produce the electrode patterns. Since lowering the electrode width always increases the output, choosing the fabrication process is a matter of cost consideration and not determined by an optimization criterion.

The AT&T Model

As a final demonstration of the optimization method, consider the predictions for the AT&T motor. From the electrode inner radius and width given in the patent description, the number of electrode groups is calculated to be 262. In Figure 62, the torque for the initial rotor position is given for the presumed number of electrode groups and for three lesser values. For this model, the potential is set at 65 volts as defined in the patent. Clearly, the trend towards the optimum indicates a smaller number of groups is best. Also, without having reached the optimum, the torque output for 230 groups with radial electrodes is over twice the output for 262 groups with rectangular electrodes. This example alone justifies the need for optimization of the electrode pattern.

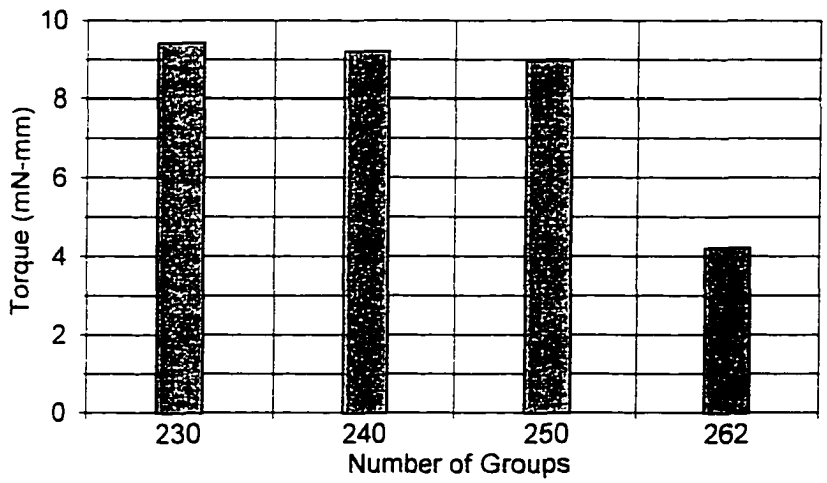

Figure 62 Torque Data for the AT&T Model

CONCLUSION

Optimization of the electrode pattern of a variable capacitance electrostatic motor results in maximizing the output. The number of electrode groups is the main parameter to consider for the optimization process. The shape angle affects the optimum design by a small percentage yet is necessary to insure peak performance. Other considerations such as minimizing the stator to rotor gap and maximizing the dielectric constants apply generally and thus are held as constants throughout the optimization process of a single motor design.

The example given in Chapter 5 shows that with modern microfabrication methods an electrostatic motor can yield greater torque output than an electromagnetic motor of the same size. Also, with the inclusion of the modified electrode charge pattern described in Chapter 6, the predicted output can be increased by an additional 30%.

The numerical investigation has demonstrated the viability of an electrostatic motor as a competitor for its electromagnetic counterpart. With the information provided herein, experimentation to prove the value of electrostatic designs is now warranted.

REFERENCES

1. A. D. Moore. Electrostatics and Its Applications, John Wiley and Sons. NY. 1973. pp. 133-138.

2. Oleg Jefimenko, Electrostatic Motors, Electret Scientific Company. Star City. West Virginian. 1973.

3. B. Bollée. Electrostatic Motors, Philips Technical Review. Vol. 30. No. 6/7. 1969. pp.178-194.

4. J. H. Staudte. Electrostatic Motor, United States Patent. 3.629.624. December 21. 1971.

5. Ferriss et al. Electrostatic Motor. United States Patent, 3.951.000. April 20. 1976.

6. Gary Stix. Micron Machinations, Scientific American. Nov. 1992. pp. 106-117.

7. W. S. N. Trimmer and K. J. Gabriel. Design Considerations for a Practical Electrostatic Micro-motor, Sensors and Actuators. 11. 1987. pp. 189-206.

8. Gabriel et al. Micro-Electrostatic Motor. United States Patent. 4.754.185. June 28. 1988.

9. S. Bart and J. Lang, Electroquasistatic Induction Motors. MEMS 1989. pp. 7-12.

10. R. Mahadevan. Analytical Modeling of Electrostatic Structures. IEEE Press. 1990. pp.120-127.

11. S. Kumar and D. Cho. A Perturbation Method for Calculating the Capacitance of Electrostatic Motors. IEEE Press, 1990, pp.27-33.

12. S. Egawa and T. Higuchi, Multi-layered Electrostatic Film Actuator. MEMS 1990. pp. 166-171.

13. S. Egawa et al, Film Actuators: Planar Electrostatic Surface-Drive Actuators. MEMS 1991, pp. 9-14.

14. T. Niino et al. Development of an Electrostatic Actuator Exceeding 10N Propulsive Force. MEMS 1992. pp. 122-127.

15. T. Niino et al. High-Power and High-Efficiency Electrostatic Actuator. MEMS 1993. pp. 236-241.

16. T. Niino et al. Electrostatic Artificial Muscle: Compact High-Power Linear Actuators with Multi-Layer Structures, MEMS 1994, pp. 130-135.

17. C. L. Rambin et al, A Solution Procedure for the Electrostatic Drive Analysis of Rotary and Linear Microactuators, ASME Micromechanical Systems, DSC-Vol. 46, Nov. 1993, pp.97-105.

18. B. C. Rao et al, Finite Element and Analytical Modeling of a Surface-Driven Electrostatic Micromotor, ASME, Nov. 1994.

19. R. X. Gao et al. Design and Performance Evaluation of Linear and Rotary Surface-Driven Electrostatic Micromotors, International IEEE IACC 95, Taipei, May 23, 1995, pp. 572-577.

20. Gary Chamberlain, Conducting Polymers, Design News, Jan. 21, 1991, pp. 60-66.

21. American Laubscher Corporation, Farmingdale, New York

22. ALCATEL Corporation, San Jose, California

23. Aries Electronics Incorporated, Frenchtown, New Jersey

24. Dynamics Research Corporation, Wilmington, Massachusetts

25.Y. B. Yildir and B. W. Klimpke, Calculation of Transmission Line Parameters with the Boundary Element Method, ANTEM 1988, Winnipeg, Manitoba, August 10-12, 1989, pp. 1-8.

26. Y. B. Yildir, Three-Dimensional Electrostatic Field Analysis on the Microcomputer, IWCA 1989 Coil Winding Proceedings, September 25, 1989, pp. 59-65.

27. S. R. Knutson et al, PC-Based Electrostatic Field Calculation Techniques, The 12th Annual Ideas in Science and Electronics Exposition / Symposium, May 10, 1991, pp. 166-171.

28. Integrated Engineering Software, Inc., Manitoba, Canada.

29. Micro Mo Electronics, Inc., Clearwater, Florida.

IMAGE EVALUATION TEST TARGET (QA-3)

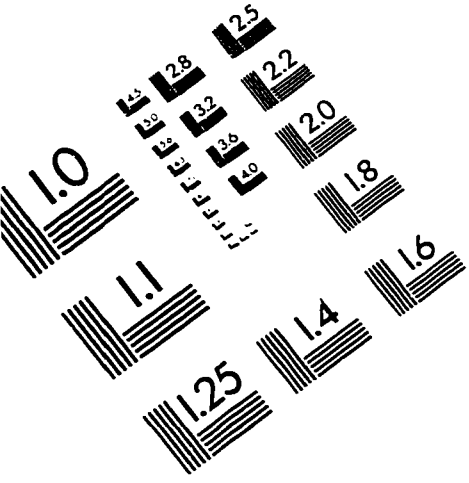

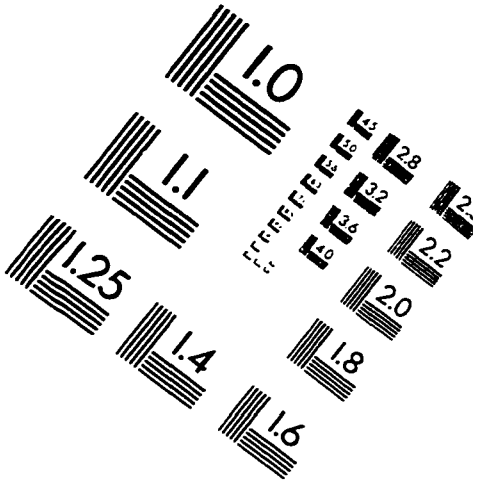

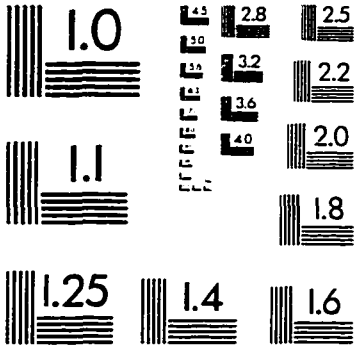

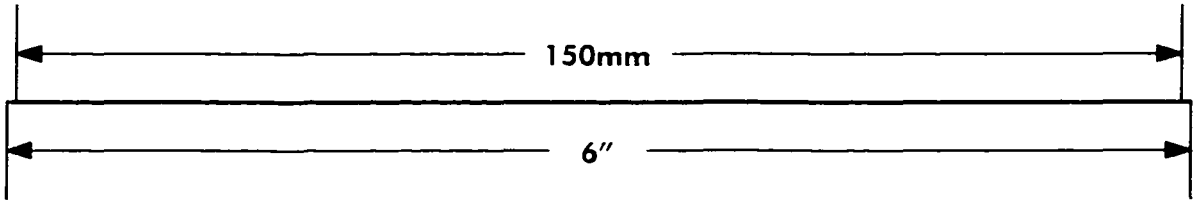

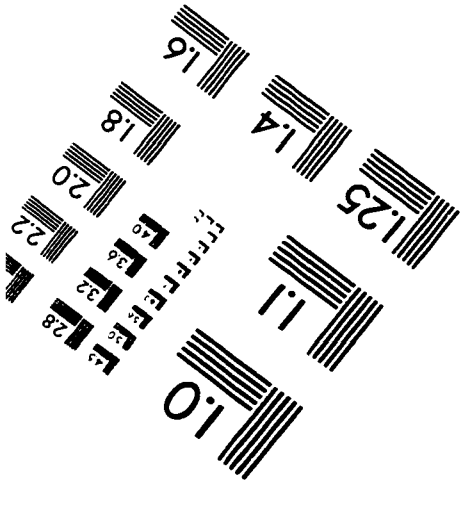

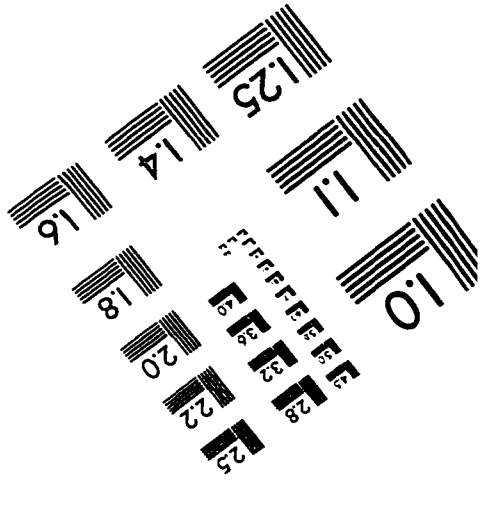

APPLIED IMAGE, Inc
1653 East Main Street
Rochester, NY 14609 USA
Phone: 716/482-0300
Fax: 716/288-5989